POLITECNICO DI TORINO

Master's degree course in Nanotechnologies for ICTs

Master's Thesis

Thermal laser process of thin silicon carbide deposited by PECVD

Relatori
Prof. Luciano Scaltrito
Prof. Sergio Ferrero

Tutor
Daniele Arduino

Candidato
Francesco Iozzi
Matr. 282905

April 2024

To my Family

Index

Acknowledgements

It is my duty to dedicate this space of my work to the people who contributed, with their tireless support, to the realization of this work.

First, a special thanks to my supervisor Luciano Scaltrito and my co-supervisor Sergio Ferrero for their immense patience, for their indispensable advice and knowledge transmitted during the writing of the essay.

Special thanks to my family. Words cannot express how much I am grateful to my mother and father for all the sacrifices they made for me. Your encouragement was what most supported me in achieving this goal, giving me strength and courage to go through difficult periods.

A huge thanks to my tutor Daniele Arduino for the help given me during the writing of the thesis work and its immense availability.

To my friends, thank you for being my accomplices, each in their own way, in this intense and exciting journey, for better or for worse.

There are so many memories running through my head that it's impossible to find the right words to honour them. This will be done by my emotions and smiles which together blend into a wealth of sincere affection and gratitude for all of you.

Without all of you I would never have done it, thank you.

Summary

The activity transcribed in this thesis was carried out in collaboration with the company Microla Optoelectronics.
Microla is specialized in the use of laser sources both for industrial applications and to carry out in-depth research studies.
The work on which the thesis is based consists in analysing and characterizing the result obtained from an annealing process carried out by means of a laser source on a sample of a thin film amorphous Silicon Carbide deposited on SiO2 thin film on Silicon substrate.
This includes the realization of an optical setup to develop the process of thermal annealing of the thin film amorphous SiC sample; the obtained result has been then analysed by characterization techniques such as Raman spectroscopy, X-ray Diffraction spectroscopy and Transmission Electron Microscopy to verify whether the crystallization of the layer on which thermal annealing was carried out was successful.
The research to this end is particularly innovative, given the great absence of scientific material available on the subject in question.
The organization of the thesis work is divided into the following 5 chapters:

1. In the *first chapter*, a description of Silicon Carbide and the Thermal annealing process is provided.
2. In the *second chapter*, the characterization techniques used to carry out the measurements are introduced, the results of which will be discussed in a subsequent chapter.
3. In the *third chapter*, the work carried out on the various samples is described, with a focus on the differences found between the results obtained with a green laser source and those found by annealing with an UV laser source. The latter is extremely necessary because the green laser provides a fixed pulse width which is not what is required to obtain a good and uniform annealing and consequently an achievable crystallization of the topmost layer of the sample.

4. The fourth chapter is fully dedicated to the procedure required to obtain the lamella, a single thin sheet from the annealed sample, achieved with FIB, the characterization done with the TEM instrument and lastly a discussion about the obtained results.
5. The fifth chapter resumes the entire research with a focus on the achieved results, presents the conclusions about the quality of the thesis work and the future perspectives.

Chapter 1: SiC and Thermal Annealing

1.1 Introduction

The focus of this chapter is to give a clear delineation of the material used for the entire work thesis time, which is Silicon Carbide, describing it from a physical, chemical, electrical and an applicative point of view. Defining silicon carbide's polytypes and the difference between the amorphous and crystalline phases of the material is also essential to get a clear view of how the material represents indeed a turning point for many technological applications.

Another important concept that will be taken into consideration is the thermal process that leads to the change from the amorphous phase to the crystalline phase of SiC, crucial aspect of this thesis work.

Silicon Carbide (SiC) represents a beacon of innovation and promise, embodying the transformative potential of advanced materials in modern technology. Having a unique combination of exceptional properties, SiC represents a versatile material with a wide range of applications across various fields, going from electronics and automotive to industrial and aerospace applications.

Silicon Carbide was firstly utilized back in the 19th century when chemists were trying to have a better understanding of the nature of carbon compounds. However, SiC began to garner significant attention as a material only in the last 30 years and so, extensive research has been done on SiC to unlock its potential and pave the way for groundbreaking innovations.

1.2 SiC Semiconductor

Chemically, Silicon Carbide is a compound semiconductor composed of silicon and carbo atoms arranged in a crystalline lattice structure which is akin to that of diamond. Unlike diamond though, SiC presents an alternating silicon and carbon atoms in a 1:1 ratio. This unique arrangement grants SiC a vast array of properties.

The more remarkable ones are:

- **High Hardness**: Silicon Carbide boasts an outstanding hardness which is naturally second only to diamond, making it a good candidate for abrasive applications like polishing or grinding.
- **High Thermal Conductivity**: SiC can efficiently dissipates heat, having a thermal conductivity comparable to that of copper, making it an ideal candidate for thermal management systems and obviously electronic devices.
- **Wide Bandgap Semiconductor**: Silicon Carbide's bandgap exceeds that of traditional semiconductors such as Silicon and Gallium Arsenide. This trait enables SiC-based devices to operate at higher temperatures, voltages, and frequencies, offering enhanced efficiency, reliability and performance in power electronics or high frequency applications.
- **Chemical Inertness**: SiC exhibits excellent resistance to chemical corrosion. This makes a good choice when requiring a material that can withstand aggressive environments, where typically other materials would degrade.

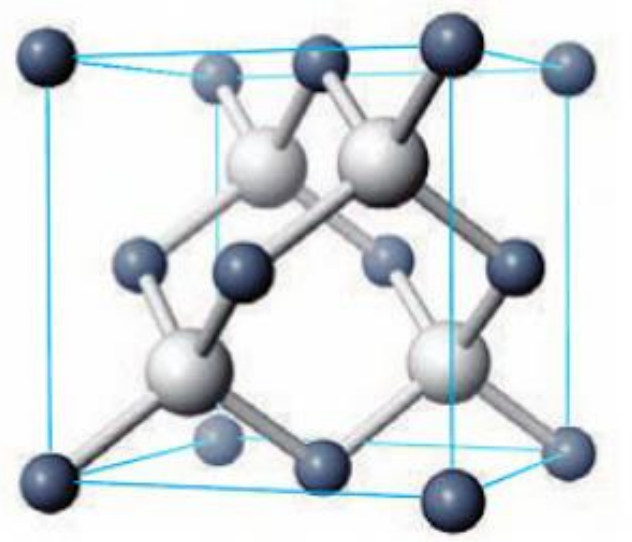

Fig. 1: *Unit cell of SiC.*

Many compound materials present polymorphism which is the existence of more than a single crystalline structure that the material could have.

Silicon Carbide presents more than 250 polymorphisms that contain various amorphous phases and a family of crystalline structures called polytypes.
Polytypes are formed by stacking SiC molecules on top of each other in a certain order; in fact, the stacking order between succeeding double layers of C and Si atoms determines the difference between polytypes.
The most common polytypes include 3C, 4H and 6H. The letters denote the overall lattice type as being hexagonal(H), cubic(C) or even rhombohedral (R).
In SiC device research the most used polytypes are two: 6H-SiC also known as alpha-SiC and 4H-SiC.
6H-SiC was used since before the 90's but nowadays 4H-SiC has become the dominant polytype thanks to the fact that the charge-carrier mobilities in 4H-SiC are identical along the two planes of the semiconductor, whereas the 6H-SiC polytype exhibits anisotropy.

Each polytype of silicon carbide has distinct properties that make it suitable for different applications:

1. 4H-SiC: This polytype is widely used in high-power electronic devices, such as power MOSFETs (Metal-Oxide-Semiconductor Field-Effect Transistors), Schottky diodes, and high-frequency RF (Radio Frequency) devices. Its high electron mobility, high thermal conductivity, and wide bandgap make it well-suited for applications requiring high-power operation, high-temperature stability, and high-frequency operation.

2. 6H-SiC: Similar to 4H-SiC, 6H-SiC is used in high-power electronic devices, particularly in applications requiring high voltage operation and high-temperature stability. It is also utilized in certain sensor applications and as a substrate for epitaxial growth of other semiconductor materials.

3. 3C-SiC: While less common in high-power electronic devices, 3C-SiC has advantages in its compatibility with silicon-based technology. It can be grown on silicon substrates, allowing for the integration of SiC devices with existing

silicon-based integrated circuits. This makes it suitable for applications such as integrated circuits, MEMS (Micro-Electro-Mechanical Systems), and sensors.

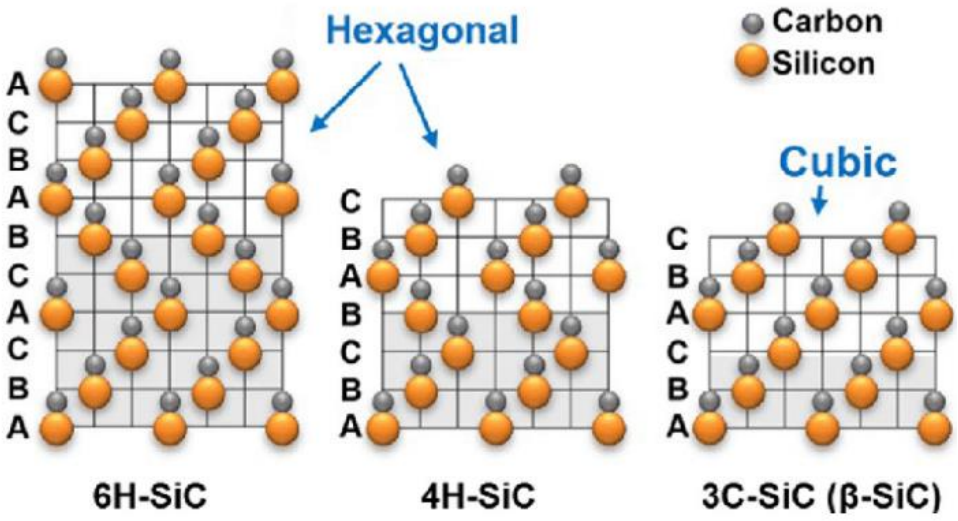

Fig. 2: *Stacking sequence of 6H-, 4H- and 3C-SiC.*

1.3 SiC Crystallization

Since the aim of the thesis is to achieve the crystallization of an amorphous sample of SiC a brief and clear description of these two phases is indeed necessary.

Amorphous silicon carbide (a-SiC) lacks long-range order in its atomic arrangement, exhibiting a disordered and random structure. This lack of crystallinity imparts distinctive properties to amorphous SiC, including transparency in the visible and infrared spectra, flexibility, and ease of attainability through processing.

A-SiC is typically produced through techniques such as chemical vapor deposition (CVD) or sputtering, where precursor gases are deposited onto substrates at temperatures around

400 degrees, leading to the formation of a non-crystalline film. The absence of grain boundaries in amorphous SiC results in isotropic properties, making it suitable for applications requiring uniformity and isotropy such as protective coatings, optical components, and thin-film electronics.

Due to its disordered atomic structure, amorphous silicon carbide exhibits unique electronic properties, including tuneable bandgaps and defect states.
These properties find applications in photovoltaics, sensors, and optoelectronic devices, where precise control over electronic properties is necessary.
In contrast to its amorphous counterpart, crystalline silicon carbide (c-SiC) boasts an ordered and well-defined atomic structure, characterized by the arrangement of silicon and carbon atoms in a periodic lattice. This crystalline arrangement grants to c-SiC properties such as high thermal conductivity, exceptional hardness, and superior mechanical strength. The crystalline nature of SiC facilitates the formation of well-defined grain boundaries, granting unique electrical and optical properties.
Within c-SiC, various polytypes exist and I already discussed a few of them. Each of these polytypes possesses distinct crystal structures and properties. The choice of polytype significantly influences the material's characteristics and suitability for specific applications. For instance, 4H-SiC exhibits superior electrical properties, making it ideal for high-power electronic devices, while 6H-SiC finds utility in high-temperature applications due to its thermal stability.

Parameter	2H-SiC	4H-SiC	6H-SiC	3C-SiC
Stacking order	AB	ABCB	ABCACB	ABC
Jagodzinskii notation	h	hc	hcc	c
Percentage 'hexagonality', γ (%)	100	50	33	0
Lattice constant (Å)	$a = 3.076$ $c = 5.048$	$a = 3.073$ $c = 10.053$	$a = 3.08$ $c = 15.117$	4.34
Band gap (eV)	3.33	3.26	3.0	2.39
Thermal conductivity (W cm^{-1} °C^{-1})		3–4	3–4	3–4
Critical breakdown field strength, E_{cr} (MV cm^{-1})		2–3	2–3	>1.5
Electron mobility, μ_n (cm^2 V^{-1} s^{-1}) (300 K)		⩽850	⩽450	⩽1000
Saturation rate, V_s ($\times 10^7$ cm s^{-1})		2	2	2.7
Hole mobility, μ_p (cm^2 V^{-1} s^{-1}) (300 K)		⩽120	⩽100	⩽40

Fig. 3: *Main parameters of different SiC polytypes*

The crystalline nature of SiC renders it well-suited for applications requiring precise control over material properties, such as semiconductor manufacturing, abrasive machining, and high-temperature electronics. Its well-defined structure facilitates the fabrication of intricate

devices with tailored electronical, mechanical, and optical characteristics which contributes to its widespread adoption in modern technology.
The main aspects of both phases can be resumed as follows:

1. Crystalline SiC possesses a periodic lattice structure, whereas amorphous SiC lacks long-range order.
2. C-SiC exhibits superior mechanical, thermal, and electrical properties, while a-SiC offers transparency, flexibility, and isotropy.
3. C-SiC is very utilized in high-performance electronics, abrasives, and high-temperature applications while a-SiC is employed in thin-film electronics, optical coatings, and sensors.

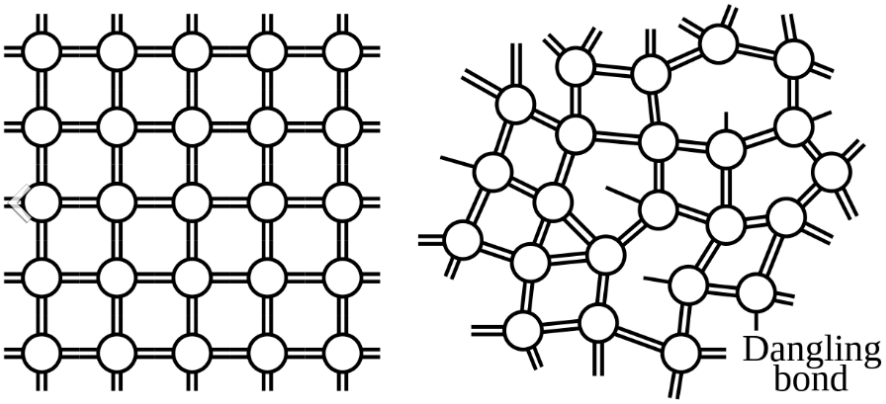

Fig. 4: *Schematic structures of Crystalline silicon on the left and amorphous silicon on the right.*

In conclusion, the disparity between a-SiC and c-SiC carbide lies at the heart of their distinct properties and applications. While crystalline SiC offers unparalleled mechanical and electronic performance, amorphous SiC provides unique advantages in terms of transparency, flexibility, and isotropy. Both forms play a key role across various industries, contributing to the advancement of technology and innovation. Understanding their dissimilarity enables tailored utilization, harnessing the full potential of silicon carbide in diverse applications.

Transforming silicon carbide (SiC) from its amorphous state to a crystalline form involves several techniques, each offering distinct advantages and suited to specific applications.

While the process itself can be complex, several key methods stand out for their efficiency in achieving this transformation.
Some common techniques are:

- **Annealing**: It involves heating the amorphous SiC material to high temperatures under controlled conditions. This process ensures the rearrangement of atoms, allowing them to form a crystalline structure. Annealing can be performed using various methods such as furnace annealing, rapid thermal annealing (RTA), or laser annealing. Each of these methods offer different temperature profiles and heating rates. Laser annealing is the heart of this part and will be discussed later.

- **Solid-phase Crystallization**: Solid phase crystallization of amorphous silicon proceeds via random nucleation and growth of crystalline nuclei. Low pressure chemical vapor deposition from disilane serves to deposit amorphous Si films at 450°C, which are then crystallized at temperatures around 600°C.

- **Sequential Lateral Solidification:** The sequential lateral solidification (SLS) process is an excimer-laser projection-based scheme for crystallization of thin films on amorphous substrates. This method grants the production of a wide range of microstructures by manipulating the grain boundary's placement within the crystallized material.

Let us focus now on the technique which represents a pivotal point of this work of thesis, Annealing, while introducing right after the precise technique used to achieve the transformation from a-SiC into its crystalline form, Laser Annealing.

Annealing is a heat treatment process used to modify the properties of materials, typically metals and alloys, by subjecting them to controlled heating and cooling cycles. The goal of annealing is to relieve internal stresses, improve ductility, reduce hardness, and enhance other desirable characteristics without altering the material's chemical composition.

The annealing procedure usually involves the following three steps:

1. **Heating**: The material is heated to a specific temperature, known as the annealing temperature, which varies depending on the material type and desired outcomes. During heating, the material's atoms gain kinetic energy, causing them to vibrate more vigorously and facilitating the movement of defects such as dislocations.

2. **Soaking**: Once the material reaches the annealing temperature, it is held at that temperature for a predetermined period, allowing for uniform heating throughout the material. This soaking period is crucial for enabling the desired structural changes to occur, such as the rearrangement of atoms and the reduction of internal stresses.

3. **Cooling**: After the soaking period, the material is gradually cooled at a controlled rate. The cooling rate is critical and can significantly impact the final properties of the material. Slow cooling rates are often employed to minimize the formation of new internal stresses and achieve a more uniform microstructure.

The annealing process favours the rearrangement of atoms within the crystal lattice of the material reducing defects and improving the material's overall structure and properties. The three key mechanisms involved in annealing are:

1. **Recovery**: At lower temperatures during annealing, recovery processes occur where dislocations move and rearrange themselves, reducing their density within the material. This helps relieve internal stresses and increase the material's ductility.

2. **Recrystallization**: As the temperature increases further, recrystallization begins to take place, wherein new, strain-free grains nucleate and grow within the material. This process results in a more uniform grain structure, improved mechanical properties, and increased resistance to deformation.

3. **Grain Growth**: Continuously heating can lead to grain growth where already existing grains within the material grow. While excessive grain growth can sometimes be detrimental to material properties, controlled grain growth can be beneficial for achieving specific characteristics, such as increased strength or improved electrical conductivity.

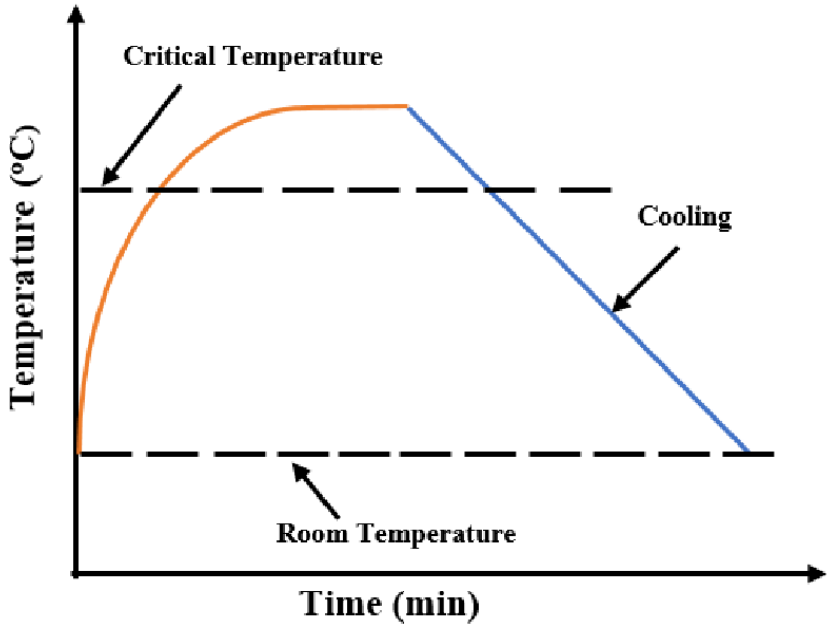

Fig. 5: *Schematic diagram of an annealing treatment process.*

Overall, the annealing process is a versatile and widely used technique for tailoring the properties of materials to meet specific application requirements. By carefully controlling the heating, soaking, and cooling parameters, engineers can achieve a wide range of desired outcomes, from softening metals for easier machining to enhancing the electrical conductivity of semiconductors.

1.4 Laser Annealing

The objective of this final part of the first chapter is to introduce and investigate a typical laser annealing process that targets a sample material.

Laser annealing is a sophisticated technique employed in materials science and engineering to modify the properties of surfaces or thin films through the precise application of intense laser energy. Unlike conventional annealing methods that involve heating entire materials to high temperatures, laser annealing offers a highly localized and controlled approach. This helps minimizing thermal impact on the surrounding areas of the sample.

In laser annealing, a focused laser beam is directed onto the material surface, generating rapid heating and subsequent cooling within a fraction of a second. This rapid thermal process induces structural changes in the material, such as crystallization, recrystallization, or phase transformations, depending on the specific properties desired.
One of the key advantages of laser annealing is its ability to achieve ultra-fast processing speeds with exceptional precision, making it ideal for applications where high throughput and fine-tuned control is essential. This technique finds widespread use in various industries, including semiconductor manufacturing, photovoltaics, display technology, and biomedical engineering, among others.

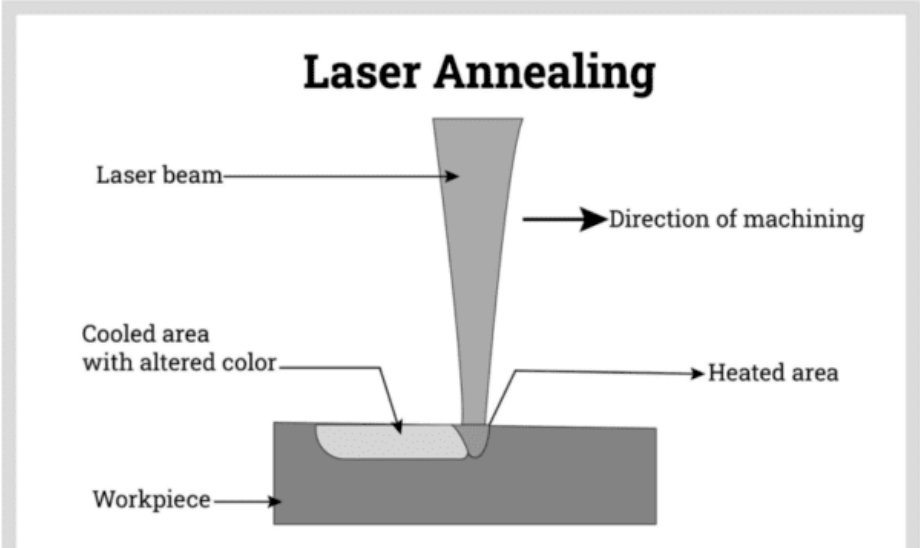

Fig. 6: *Schematic diagram of a laser annealing process.*

Laser annealing employs various types of lasers depending on the specific requirements of the application. The main sources of laser are:

1. **Excimer Lasers**: Excimer lasers, such as those emitting ultraviolet (UV) light, are frequently used in semiconductor manufacturing for annealing processes. Their short wavelengths and high photon energy make them suitable for precise material modification without excessive heat buildup.
2. **Nd: YAG**: Nd: YAG (neodymium-doped yttrium aluminium garnet) lasers emit infrared light and are valued for their versatility and reliability. They find applications in annealing processes requiring deeper penetration into materials, such as annealing of thin metallic films.

3. **CO2 Lasers**: CO2 lasers emit infrared light and are known for their ability to deliver high-power beams over large areas. While less common for laser annealing compared to other types, CO2 lasers find niche applications in annealing processes requiring uniform heating across large surface areas, such as annealing of glass substrates.

4. **Diode Lasers**: Diode lasers offer compactness, efficiency, and wavelength flexibility making them suitable for various annealing applications, particularly in the field of microelectronics and photonics. They are often utilized for localized annealing processes where precise control is key.

The choice of laser depends on factors such as annealing speed, material composition and thickness.
During the work thesis the laser sources that were used to perform annealing are:

- **532 nm Vlase model 2109-TFS2 Fiber Laser**: A fiber laser is a type of laser that utilizes optical fibers as the gain medium to amplify light. Unlike traditional gas or crystal lasers, which use a solid, liquid, or gas as the active medium, fiber lasers use a doped optical fiber as the gain medium. The fiber is typically doped with rare-earth elements such as erbium, ytterbium, or neodymium, which provide the necessary energy levels for laser action.

- **Sol model 4W 355 nm UV Laser:**

Both lasers' specifications and descriptions will be given in chapter 3.

Chapter 2: Characterization Techniques

2.1 Introduction

In this chapter we will focus on the main characterization techniques that were used during the final steps regarding the analysis of the samples that underwent the process of laser annealing.

The focus will mainly be on the theoretical description of the techniques while a separate chapter will include the analysis and discussion of the obtained results.

The characterization techniques that were used in a chronological order are:

1. Optical Microscopy
2. X-ray Diffraction
3. Raman Spectroscopy
4. Scanning Electron Microscopy
5. Transmission Electron Microscopy

2.2 Optical Microscopy

Optical Microscopy stands as one of the most fundamental and versatile tools in the scientific arsenal, enabling researchers to explore the intricate details of the microscopic world with unparalleled clarity and precision.

A typical setup of an optical microscope consists of several key components designed to produce magnified and illuminated images of samples; they are:

1. **Base and Frame**: The base provides stability and support for the entire microscope, while the frame holds the optical components in place. The base and frame are usually constructed from sturdy materials, such as metal or plastic, to ensure rigidity and durability.

2. **Illumination System**: The illumination system provides light to illuminate the sample being observed. Common types of illumination sources include halogen lamps, LED lights, or fluorescence lamps, depending on the specific requirements of the observation. The light source is often located in the base of the microscope and directed upward through the sample.
3. **Condenser**: The condenser is an optical component located beneath the stage that focuses and directs light onto the sample. It typically consists of lenses and an adjustable diaphragm to control the intensity and angle of illumination. The condenser helps to optimize the contrast and brightness of the sample image.

4. **Stage**: The stage is a platform where the sample is placed for observation. It may include mechanical controls, such as knobs or motorized actuators, to move the sample in different directions (x, y, and z axes) for precise positioning and focusing. Some stages also incorporate heating or cooling elements to control the temperature of the sample during observation.

5. **Objective Lenses**: Objective lenses are located near the bottom of the microscope and are responsible for magnifying the image of the sample. Microscopes typically have multiple objective lenses with different magnification levels (e.g., 4x, 10x, 40x, 100x) that can be rotated into position for observation. The numerical aperture (NA) of the objective lenses determines their resolving power and light-gathering ability.

6. **Ocular (Eyepiece)**: The ocular, or eyepiece, is located near the top of the microscope and is used to view the magnified image of the sample. Oculars typically have a magnification power of 10x and may contain additional optics, such as reticules or graticules, for measuring distances or angles in the sample. Some microscopes may also include a binocular viewing head with two oculars for stereoscopic observation.

7. **Adjustment Mechanisms**: Microscopes are equipped with various adjustment mechanisms to focus and align the optical components for optimal image quality. Coarse focus knobs allow rapid movement of the stage along the z-axis to bring the sample into approximate focus. Fine focus knobs provide finer adjustments to achieve precise focus and clarity in the image. Other adjustment mechanisms may include dioptre adjustment for the oculars, stage lock to prevent sample movement, and condenser height adjustment.

8. **Camera and Imaging System (Optional)**: Some optical microscopes may be equipped with a camera and imaging system for capturing digital images and videos of the sample. Cameras can be mounted on the microscope's viewing head or connected externally via a camera port. Imaging software allows users to manipulate and analyse the captured images, as well as store and share data electronically.

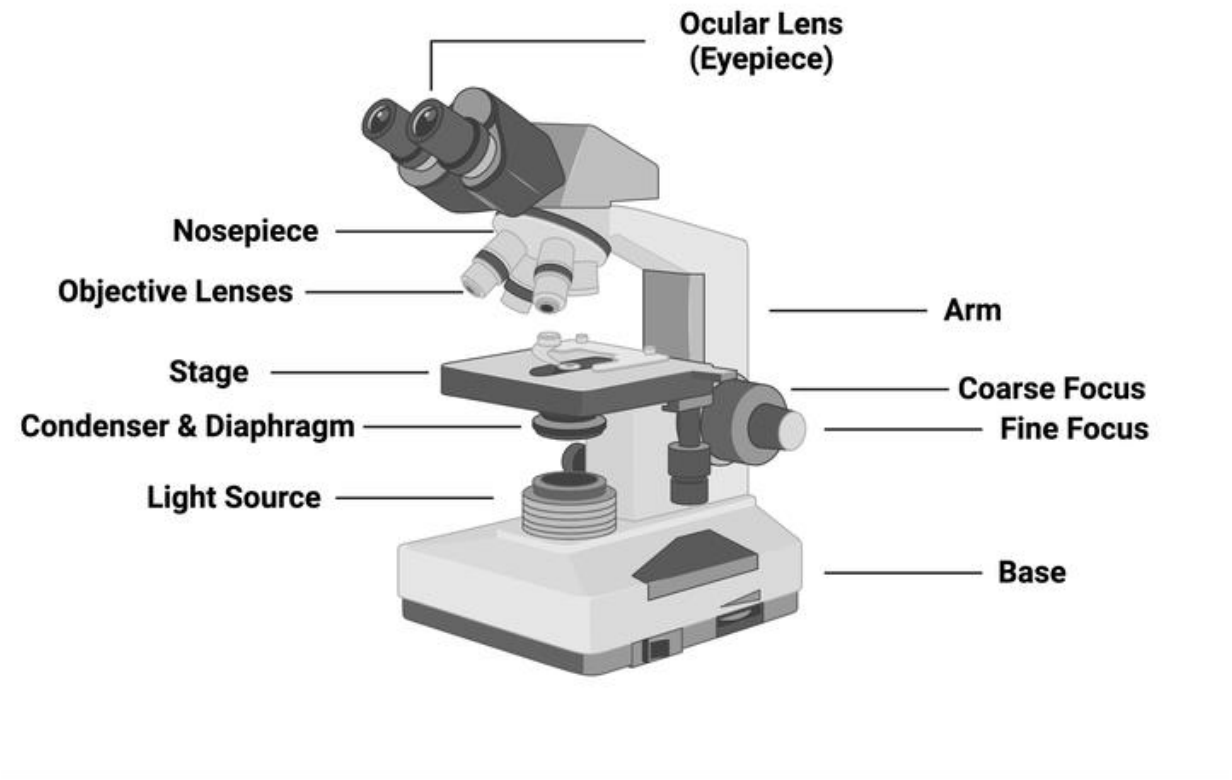

Fig. 7: *Diagram of a compound light microscope with labels.*

Overall, the typical setup of an optical microscope consists of a combination of these components, each playing a crucial role in the production of high quality and magnified images of samples for observation and analysis.

The Optical microscope was the first characterization technique used to analyse the obtained results of the laser annealing process and granting an initial view of the possible outcome coming from the lasering of the SiC sample.
The analysis which was done with it will be further discussed in the next chapter.

2.3 X-ray Diffraction

X-Ray Diffraction represents a cornerstone in the field of materials science, offering great insights into the atomic and molecular structure's description of crystalline solids.

The roots of X-ray diffraction can be traced back to the early 20th century, marked by the seminal discoveries of father-and-son duo William Henry Bragg and William Lawrence Bragg. In 1912, the Braggs formulated Bragg's Law, which describes the relationship between the angles of incidence and diffraction for X-rays interacting with crystalline materials. This groundbreaking law provided a theoretical framework for understanding the diffraction phenomenon and laid the groundwork for the field of X-ray crystallography. The Braggs' pioneering work earned them the Nobel Prize in Physics in 1915, cementing their legacy as foundational figures in the history of XRD.

Throughout the early to mid-20th century, significant technological advancements propelled the development of X-ray diffraction techniques. Powder diffraction emerged as a powerful method for analysing the crystal structures of powdered materials, enabling researchers to obtain diffraction patterns that reflect the crystalline phases present in a sample. The invention of rotating-anode X-ray generators and film-based detectors facilitated the collection of high-quality diffraction data, paving the way for detailed structural analyses of diverse materials.

The advent of single crystal X-ray diffraction revolutionized the field of crystallography, allowing scientists to determine the precise atomic arrangements within individual crystalline specimens. Max von Laue's discovery of X-ray diffraction by crystals in 1912 provided the theoretical basis for single crystal analysis, while the development of Laue's photographic method by Friedrich and Knipping enabled the first experimental demonstration of crystal diffraction. Subsequent innovations, such as the precession method and the introduction of area detectors, further enhanced the accuracy and efficiency of single crystal XRD, leading to groundbreaking discoveries in structural biology, chemistry, and materials science.

As already mentioned, at the heart of X-ray diffraction lies Bragg's Law, which states that when X-rays strike a crystalline lattice at a particular angel of incidence, they undergo constructive interference if the path difference between the scattered waves from adjacent lattice planes is an integer multiple of the X-ray wavelength.

As it can be seen in fig.8, the formula provides a quantitative relationship between the angles of diffraction and the structural parameters of the crystal lattice. The diffraction phenomenon arises from the periodic arrangement of atoms within a crystalline solid, which acts as a three-dimensional diffraction grating for X-rays.

As X-rays interact with the atomic planes of the crystal lattice, they are scattered in various directions according to Bragg's Law. This results in the formation of diffraction patterns that will contain information about the crystal structure.

This way, by analysing the positions and intensities of diffraction peaks in the pattern it's possible to deduce the spacing between lattice planes and so infer the arrangement of atoms within the crystal lattice.

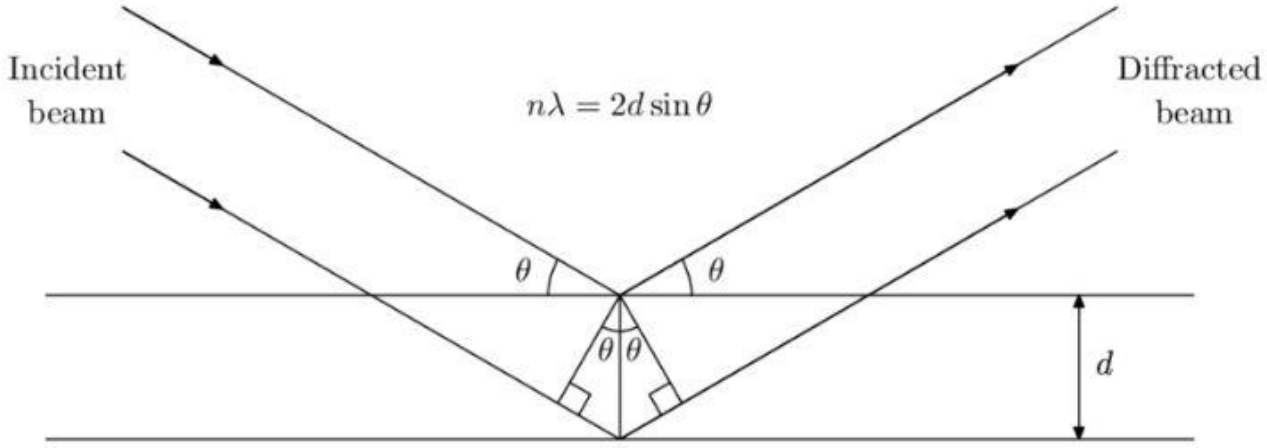

Fig. 8: *Schematic illustration of Bragg's Law.*

Finally, the interpretation of X-ray diffraction data relies on the principles of crystallography, particularly the concepts of crystal symmetry and space group analysis.

Crystals exhibit various forms of symmetry, characterized by the arrangement of atoms in repeating patterns that preserve certain geometric properties. Crystallographic symmetry operations, such as rotations, translations, and reflections, define the symmetry elements present in a crystal lattice and determine its crystallographic point group.

Space group analysis extends the concept of crystal symmetry to three-dimensional space, encompassing the combination of translational symmetry and point group symmetry to describe the overall symmetry of a crystal structure. Each space group represents a unique arrangement of symmetry elements within the crystal lattice, defining the possible orientations and configurations of atoms within the unit cell.

The incorporation of crystal symmetry and space group analysis into X-ray diffraction studies as made it possible to constrain the feasible structural models and refine the parameters of the crystal lattice to match experimental observations. This systematic approach enables the determination of accurate crystal structures from XRD data, facilitating the exploration of atomic arrangements in diverse materials and the elucidation of their physical and chemical properties.

An X-ray diffraction (XRD) setup typically consists of several key components designed to generate and analyse X-ray diffraction patterns from crystalline samples. The typical XRD setup consists of:

1. **X-ray Source**: The X-ray source emits a monochromatic beam of X-rays with a specific wavelength. Two primary types of X-ray sources are commonly utilized in XRD: laboratory-based X-ray generators and synchrotron radiation facilities. Laboratory-based X-ray generators typically employ rotating-anode or sealed-tube X-ray tubes to produce X-rays through the bombardment of a target material with high-energy electrons. These sources offer convenience and accessibility for routine diffraction experiments, allowing researchers to perform analyses in laboratory settings without the need for specialized infrastructure. However, laboratory-based sources may have limitations in terms of X-ray intensity, spectral purity, and beam divergence, which can affect the quality and resolution of diffraction data. Synchrotron radiation facilities, on the other hand, provide intense and highly collimated X-ray beams generated by accelerating electrons to relativistic speeds in circular storage rings.

Synchrotron radiation offers several advantages over laboratory-based sources, including higher brilliance, tuneable wavelength, and beam coherence, which enable advanced X-ray techniques such as high-resolution powder diffraction, small-angle X-ray scattering (SAXS), and macromolecular crystallography. Synchrotron facilities also offer specialized beamlines equipped with state-of-the-art instrumentation for specific XRD applications, allowing researchers to tailor experimental conditions to their research needs.

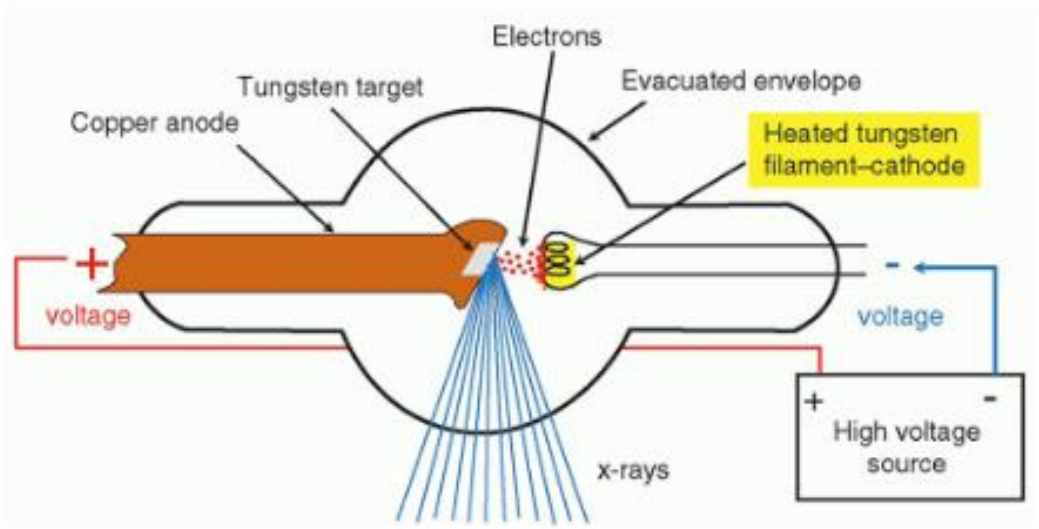

Fig. 9: *Schematic diagram of an X-ray source.*

2. **Collimation System**: The collimation system consists of X-ray optics, such as slits or mirrors, that collimate and focus the X-ray beam before it interacts with the sample. Collimation is essential for controlling the size and divergence of the X-ray beam, ensuring uniform illumination of the sample, and maximizing diffraction efficiency.

3. **Sample Stage and preparation:** The preparation of samples for X-ray diffraction analysis is a critical aspect of experimental setup, as the quality and homogeneity of the sample can significantly impact the accuracy and reliability of the diffraction

data. Sample preparation techniques vary depending on the nature of the material being studied and the desired experimental outcomes.

For powdered samples such as crystalline powders or polycrystalline materials, the sample is typically ground into a fine powder and packed into a sample holder or capillary tube for analysis. Care must be taken to ensure uniform packing and orientation of the sample to minimize preferred orientation effects and obtain representative diffraction patterns.

For single crystal samples, meticulous sample mounting and alignment are essential to ensure accurate data collection and structural analysis. Single crystals are typically mounted on a goniometer stage, which allows precise rotation and positioning of the crystal relative to the incident X-ray beam. The crystal orientation may be adjusted iteratively during data collection to optimize diffraction intensities and minimize systematic errors. In addition to sample preparation, proper handling and manipulation of samples are crucial to avoid contamination, degradation, or damage during the experimental process. Specialized equipment, such as sample handling robots or cryogenic systems, may be employed to automate sample loading and maintain sample integrity throughout the experiment.

4. **Detector system and Data acquisition:** Detection and recording of X-ray diffraction patterns rely on the performance and capabilities of detector systems used in XRD experiments. A variety of detector types are available, each with unique characteristics suited to specific applications and experimental requirements.

   Film-based detectors, such as photographic films or image plates, were historically used for capturing X-ray diffraction patterns. While these detectors offer high spatial resolution and wide dynamic range, they require manual processing and may have limited sensitivity and signal-to-noise ratio.

   Modern X-ray detectors, including semiconductor detectors (e.g., silicon strip detectors, CCD detectors) and gas-filled detectors (e.g., proportional counters, scintillation counters), offer superior sensitivity, speed, and data acquisition capabilities. Semiconductor detectors are particularly well-suited for high-resolution diffraction experiments, while gas-filled detectors excel in applications requiring high counting rates and large area coverage.

   In addition to detector selection, data acquisition systems play a critical role in recording and processing diffraction data.

   Advanced data acquisition software enables real-time monitoring of diffraction patterns, integration of diffraction intensities, and correction for instrumental effects such as background noise, detector dead-time, and beam divergence.

Fig. 10: *Image of the Empyrean XRD platform.*

Experimental techniques in X-ray diffraction encompass the selection of X-ray sources, sample preparation and handling, and the choice of detector systems and data acquisition methods. By optimizing experimental parameters and instrumentation, researchers can obtain high-quality diffraction data and extract valuable structural information from a wide range of crystalline materials.

2.4 Raman Spectroscopy

Raman spectroscopy, named after Sir C.V. Raman, who discovered the phenomenon in 1928, has evolved into a fundamental tool for chemical analysis, materials characterization, and biomedical diagnostics. This technique relies on the inelastic scattering of photons by molecules, leading to spectral shifts that reveal valuable information about molecular vibrations, structures, and compositions. The versatility of Raman spectroscopy has enabled its widespread adoption across disciplines such as chemistry, physics, biology, pharmaceuticals, and materials science.

A focus on the principles behind Raman spectroscopy is indeed needed to fully grasp the potential of this characterization technique.

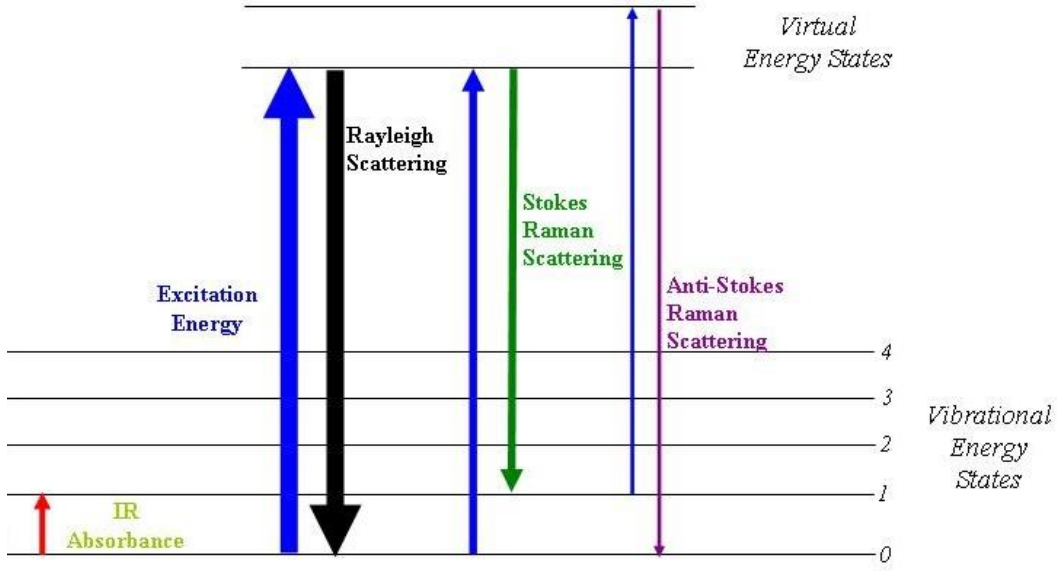

Fig. 11: *Energy levels of a molecule and Raman effect.*

The Raman effect occurs when photons interact with molecules, leading to the scattering of light with changes in energy that correspond to the vibrational and rotational transitions of the molecules. The key principles underlying Raman spectroscopy include:

1. **Inelastic Scattering**: Unlike Rayleigh scattering, where incident photons interact with molecules without any change in energy, Raman scattering involves inelastic interactions that result in the exchange of energy between the incident photons and the molecules. During Raman scattering, the scattered photons emerge with energies that are either higher (Stokes scattering) or lower (anti-Stokes scattering) than the incident photons, reflecting the energy absorbed or emitted by the molecules during their vibrational or rotational transitions.

2. **Vibrational Modes**: The Raman effect provides valuable insights into the vibrational modes of molecules, which represent the periodic motion of atoms relative to one another within the molecular structure. Each molecular bond possesses specific vibrational frequencies that correspond to the characteristic stretching, bending, and torsional motions of the atoms involved. By analysing the Raman spectra, researchers can identify these vibrational modes and elucidate the molecular composition, structure, and conformation of the sample.

3. **Raman Shift**: The energy difference between the scattered photons and the incident photons, known as the Raman shift ($\Delta\omega$), is directly proportional to the frequency of the molecular vibrations involved in the scattering process. The Raman shift is expressed in units of inverse wavelength (cm^-1) or frequency (cm^-1), allowing for the direct interpretation of vibrational frequencies in the Raman spectrum. Each peak in the Raman spectrum corresponds to a specific vibrational mode of the molecules present in the sample, providing a unique fingerprint-like signature that enables molecular identification and analysis.

4. **Selection Rules**: The intensity of Raman scattering and the selection rules governing the observed Raman bands depend on various factors, including the symmetry properties of the molecular vibrations, the polarization of the incident and scattered light, and the electronic structure of the molecules. Raman-active vibrations exhibit changes in polarizability during the scattering process, leading to observable Raman

bands in the spectrum. Conversely, vibrations that do not induce changes in polarizability (e.g., symmetric stretching modes) are Raman-inactive and do not contribute to the Raman spectrum.

5. **Raman Cross Sections**: The intensity of Raman scattering is quantified by the Raman cross section, which represents the probability of a molecule undergoing a Raman transition and emitting or absorbing photons. The Raman cross section depends on several factors, including the molecular polarizability, the electronic and vibrational states involved in the transition, and the laser wavelength used for excitation. Enhancing the Raman cross section through resonance effects, surface interactions, or multiphoton excitation techniques can significantly improve the sensitivity and detectability of Raman spectroscopy for trace analysis and surface characterization.

Focusing on the instrumentation and experimental setup of Raman spectroscopy it's possible to see how Raman spectroscopy instruments are designed to harness the Raman effect and capture the possible molecular vibrations that occur when photons interact with molecules. The typical setup includes:

1. **Laser Light Source**: Central to Raman spectroscopy is the laser, which serves as the excitation source for inducing molecular vibrations in the sample. The choice of laser wavelength is critical, as it determines the energy of the incident photons and influences the resulting Raman shifts. Commonly used lasers span a range of wavelengths, including visible (e.g., 532 nm, 785 nm) and near-infrared (e.g., 1064 nm) sources. Each wavelength offers unique advantages in terms of resolution, sensitivity, and compatibility with different sample types.

2. **Sample Holder**: Samples for Raman spectroscopy analysis are typically prepared in various forms, including solids, liquids, gases, and even biological specimens. The

sample holder must securely position the sample within the focal plane of the laser beam to ensure efficient excitation and collection of Raman scattering. Specialized sample holders may incorporate features such as temperature control, environmental isolation, and adjustable focusing to accommodate diverse experimental conditions.

3. **Spectrometer**: The spectrometer plays a crucial role in dispersing and detecting the scattered light from the sample. It consists of diffraction gratings or optical filters that separate the Raman-scattered photons based on their wavelengths, thus generating a Raman spectrum. Modern spectrometers may employ multiple detectors, such as charge-coupled devices (CCDs) or photomultiplier tubes (PMTs), to cover a wide spectral range with high sensitivity and resolution.

4. **Optics and Beam Path**: The optical components, including lenses, mirrors, and filters, are carefully arranged to manipulate the laser beam and collect the Raman signal efficiently. Beam shaping optics, such as lenses and apertures, control the beam diameter and focus to optimize the excitation intensity and spatial resolution. Additionally, optical filters are employed to suppress the residual laser light and eliminate background interference, enhancing the signal-to-noise ratio of the Raman spectra.

5. **Data Acquisition System**: Once the Raman signal is detected by the spectrometer, it is converted into electronic signals and processed by a data acquisition system. This system may include analog-to-digital converters (ADCs), amplifiers, and signal processing software for digitizing, analysing, and visualizing the Raman spectra. Advanced data processing techniques, such as baseline correction, spectral deconvolution, and multivariate analysis, are employed to extract meaningful information from complex Raman spectra and interpret the molecular characteristics of the sample.

Fig. 12: *Confocal Raman microscopy inVia Inspect by Renishaw.*

Overall, the instrumentation and experimental setup of Raman spectroscopy are meticulously designed to optimize the excitation, collection, and analysis of Raman scattering signals, enabling precise molecular characterization and chemical analysis across a diverse range of samples and applications.

During the work thesis Raman spectroscopy showed some limitations that will be discussed in the next chapter; these hindrances led the characterization work to focus on another technique, which will be discussed in the next page.

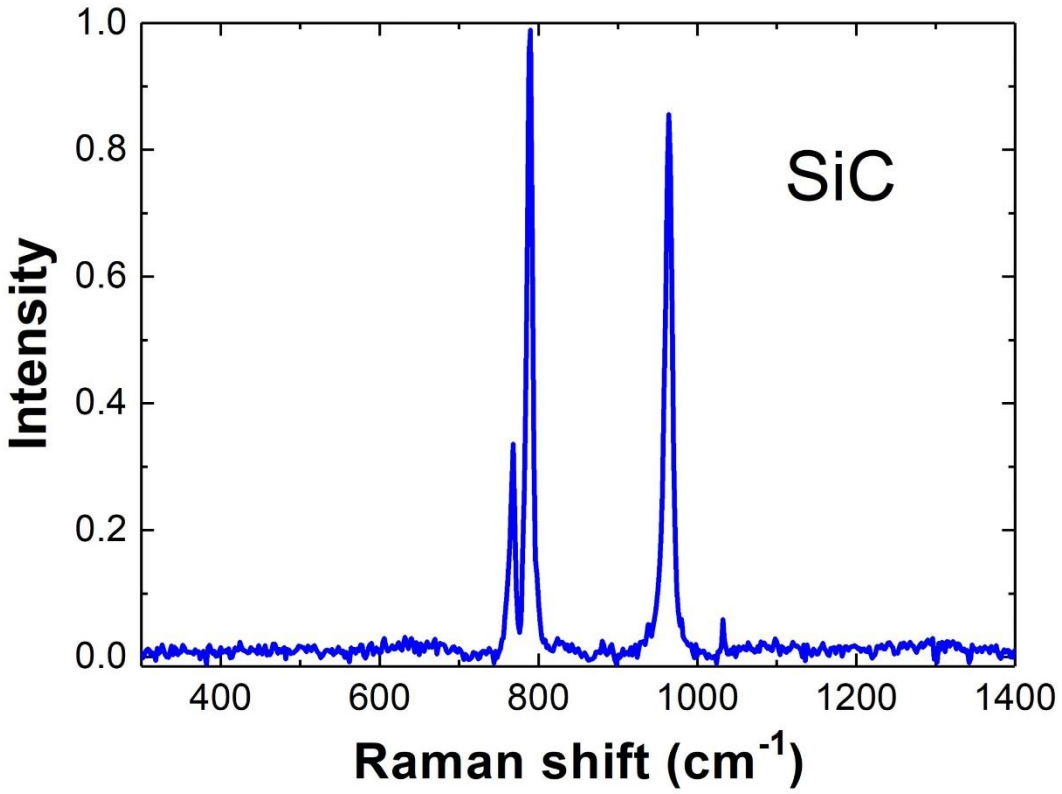

Fig. 13: *Detailed Graph of SiC Raman response.*

Microscopy has been a fundamental tool in scientific inquiry since its inception, facilitating the exploration of the microscopic world with remarkable precision. Among the plethora of microscopy techniques, Scanning Electron Microscopy (SEM) has emerged as a cornerstone, offering unparalleled insights into the morphology, composition, and structure of diverse specimens.

2.5 Scanning Electron Microscopy

Scanning Electron Microscopy unlike conventional optical microscopy, which employs visible light, utilizes electrons accelerated to high energies through a series of electromagnetic fields.

Let us focus on the main aspect of a SEM apparatus:

1. **Electron Source**: At the heart of an SEM system lies the electron source, which serves as the emitter of the electron beam. The choice of electron source significantly influences the resolution, brightness, and stability of the emitted electron beam. Commonly employed electron sources include tungsten filaments and field emission guns (FEGs). Tungsten filaments, operating under thermionic emission principles, provide a stable electron source suitable for routine imaging applications. In contrast, field emission guns utilize the field emission phenomenon, whereby electrons are emitted from a sharp tip subjected to a strong electric field, enabling higher brightness, coherence, and spatial resolution, ideal for demanding imaging and analytical tasks.

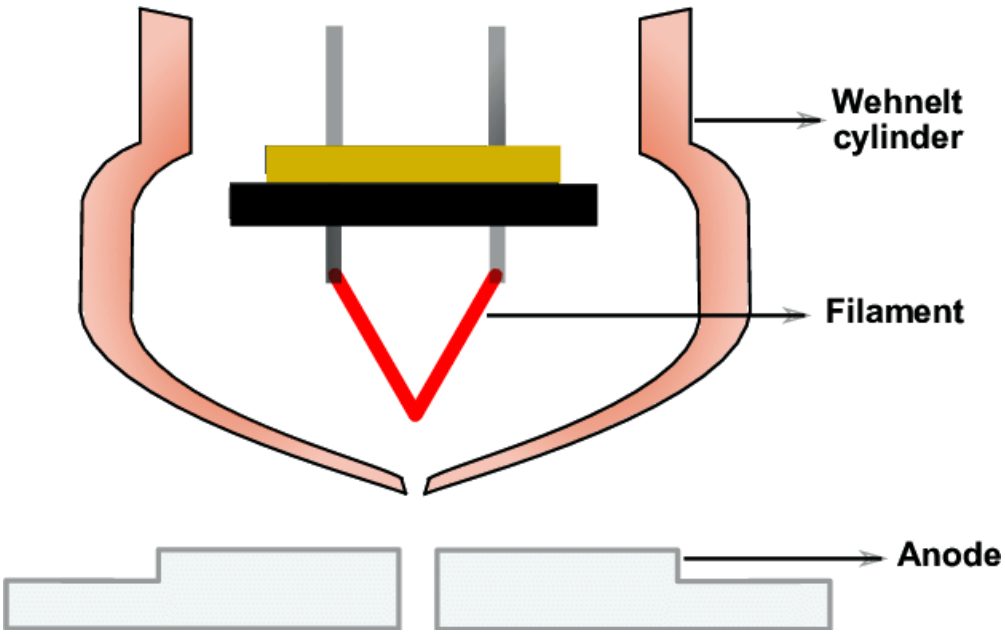

Fig. 14: *Schematic diagram of a SEM electron gun.*

2. **Electron Optics**: SEM's electron optics system comprises a series of electromagnetic lenses meticulously designed to manipulate and control the trajectory of the electron beam. Electromagnetic lenses utilize magnetic fields generated by coils or solenoids to focus, deflect, and scan the electron beam with remarkable precision. These lenses include condenser lenses for beam convergence, objective lenses for primary beam focusing, and scanning coils for beam deflection and raster scanning. The optimization of electron optics parameters, such as lens strength, working distance, and aperture size, plays a crucial role in achieving high-resolution imaging and analytical performance in SEM.

3. **Specimen Stage**: The specimen stage serves as a crucial component for positioning and manipulating specimens within the SEM chamber. Typically mounted on a motorized stage with three or more degrees of freedom, the specimen stage allows precise control over specimen positioning, tilt, rotation, and translation. Advanced specimen stages may incorporate temperature control, vacuum compatibility, and environmental chambers to accommodate a wide range of sample types and experimental conditions. The design and functionality of the specimen stage are tailored to facilitate optimal specimen imaging, characterization, and analysis, while ensuring stability, reproducibility, and ease of use.

4. **Detectors**: SEM employs a diverse array of detectors to capture and analyse the signals generated by the interaction between the electron beam and the specimen. These detectors are meticulously designed to detect specific signal types, such as secondary electrons, backscattered electrons, and characteristic X-rays, each offering unique insights into the specimen's properties. Commonly used detectors include scintillators coupled with photomultiplier tubes for secondary electron imaging, solid-state detectors for backscattered electron imaging, and energy-dispersive X-ray detectors for elemental analysis. By combining multiple detectors and signal acquisition modes, SEM can provide comprehensive information about the

specimen's morphology, composition, and structure with exceptional sensitivity and specificity.

5. **Imaging Software**: Finally, integral to SEM operation is a sophisticated imaging software, which facilitates data acquisition, processing, and visualization. This software enables real-time control of SEM parameters, such as beam energy, beam current, and imaging mode, allowing for dynamic optimization of imaging conditions. Moreover, imaging software provides advanced image processing tools for noise reduction, contrast enhancement, and three-dimensional reconstruction, enhancing the clarity and interpretability of SEM images. Additionally, modern SEM systems may integrate automation and machine learning algorithms into imaging software, enabling intelligent data analysis, pattern recognition, and feature extraction, thereby streamlining workflow, and enhancing productivity.

The SEM characterization technique was used intensively in pair with the Focused Ion Beam during the last part of the work thesis and a clearer description of its use can be found in chapter 4 of the thesis, where the samples obtained after the annealing process will be cut into thin lamellas thanks to an advanced process which combines both the already described SEM apparatus and an Ion Beam source (FIB); the latter will be specifically described chapter 4.

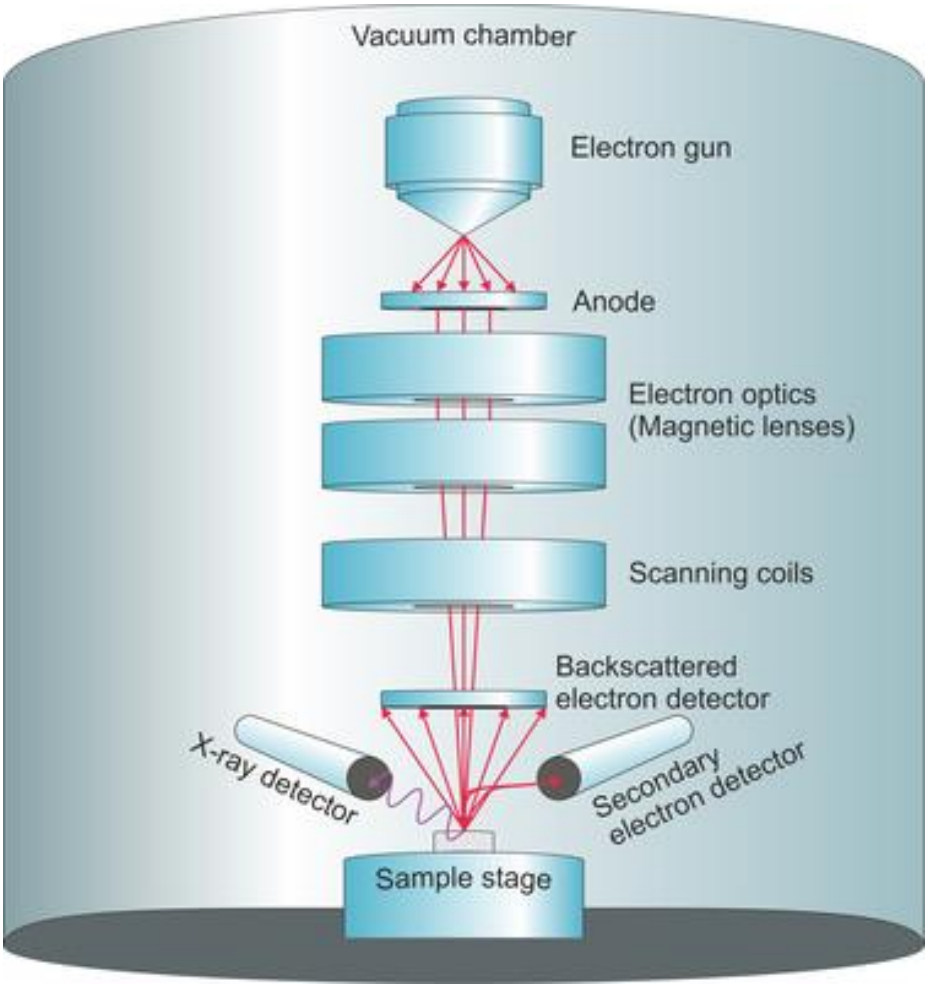

Fig. 15: *Schematic Description of a SEM apparatus.*

2.6 Transmission Electron Microscopy

Transmission Electron Microscopy enables researchers to delve into the nano-world with unprecedented clarity and resolution; since its inception, TEM has revolutionized our understanding of materials at the atomic and molecular levels, facilitating breakthroughs in various scientific domains.

As for SEM, in this part the main focus will be describing the principles that stand behind the TEM while in the fourth chapter some considerations regarding the possibility of having achieved the phase transition from the a-SiC to its crystalline dual will be made, after watching the images obtained with this last characterization technique.

The principles underlying Transmission Electron Microscopy (TEM) are rooted in the behaviour of electrons as they interact with matter. These principles dictate the operation and capabilities of TEM instruments, allowing researchers to visualize and analyse specimens at the atomic scale.

TEM is a technique which takes advantage from the electrons transmitted through the

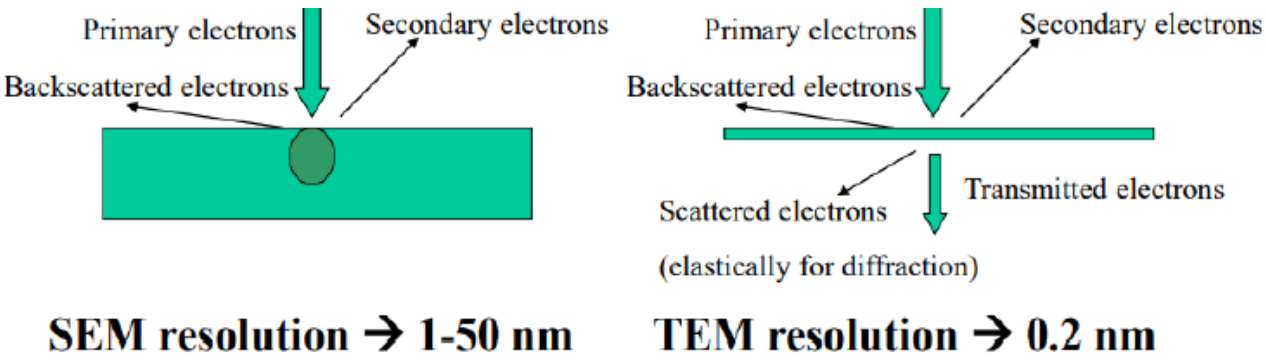

Fig. 16: *Schematic description of the types of electrons used in SEM and TEM.*

sample, differently from SEM which uses secondary and backscattered electrons.

But how is this resolution achieved? According to Louis de Broglie's hypothesis, the wavelength of a particle is inversely proportional to its momentum. This relationship is expressed by the de Broglie equation:

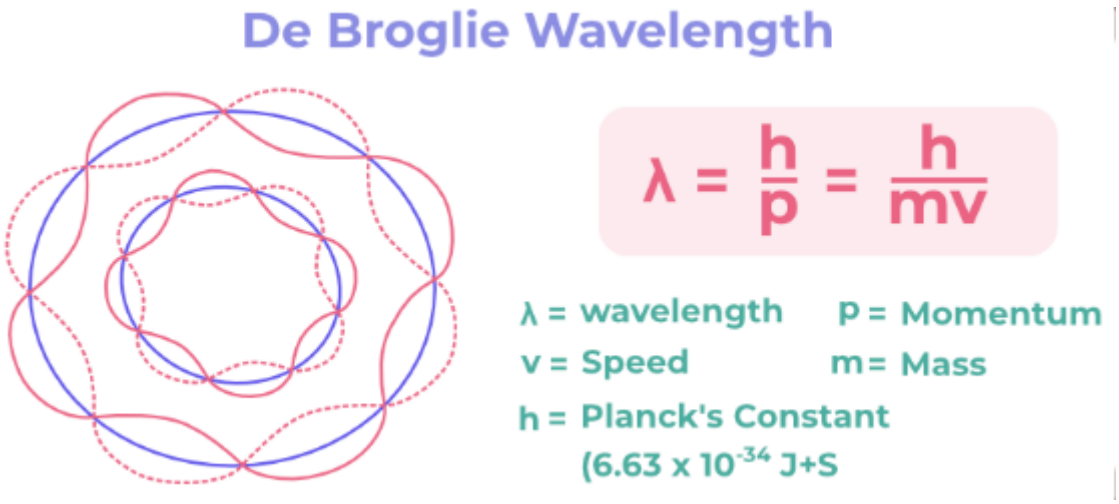

Fig. 17: *de Broglie's equation.*

In electron microscopy, electrons are accelerated to high velocities, giving them an amount of momentum that is quite significant which leads to a shortening of their wavelengths to the scale of picometers. This in turns grants to electron microscopes the possibility of achieving much higher resolution than light microscopes, which are limited by the longer wavelengths of visible light.

The TEM setup presents a few more additional features with respect to the SEM one. Let's give now a description of how it is made of:

1. **Electron Source**: TEMs typically uses a thermionic or field-emission electron gun to generate a beam of electrons. The electron gun produces a highly focused and coherent electron beam, which serves as the probe for imaging specimens.

2. **Electron Optics**: Electromagnetic lenses within the TEM column focus and manipulate the electron beam. These lenses include condenser lenses to converge the beam onto the specimen and objective lenses to focus the transmitted electrons onto a fluorescent screen or detector.

3. **Specimen Stage and Holders**: TEM specimens are typically thin sections or foils of materials mounted on specialized holders. The specimen stage allows for precise positioning and tilting of the specimen to optimize imaging conditions and acquire different views.

4. **Vacuum System**: TEMs operate under high vacuum conditions to minimize electron scattering and interactions with air molecules. The vacuum system includes pumps and seals to evacuate air from the instrument chamber and maintain a stable vacuum environment during imaging.

5. **Detectors**: Various detectors are sued to capture signals generated by the interaction of electrons with the specimen. These detectors include fluorescent screens, scintillators, and photographic films, which record the transmitted electrons to produce images with high resolution and contrast.

The key differences between TEM and SEM can be summarized into three main aspects:

- **Imaging mechanism**: In TEM, images are formed by transmitting electrons through the specimen, revealing internal structures and features. In SEM, images are generated by scanning a focused electron beam across the specimen surface and detecting signals emitted or scattered by the surface.

- **Sample preparation**: TEM specimens require extensive sample preparation, including thin sectioning and staining, to facilitate electron transmission. SEM specimens instead are typically soldi samples that may require minimal preparation, such as coating with a conductive layer to prevent charging effects that may appear during the analysis.

- **Depth of Field**: TEM imaging provides high resolution images with limited depth of field, primarily focused on thin sections of the specimen. SEM imaging instead offers greater depth of field, allowing for the visualization of 3Ds surface features on solid specimens.

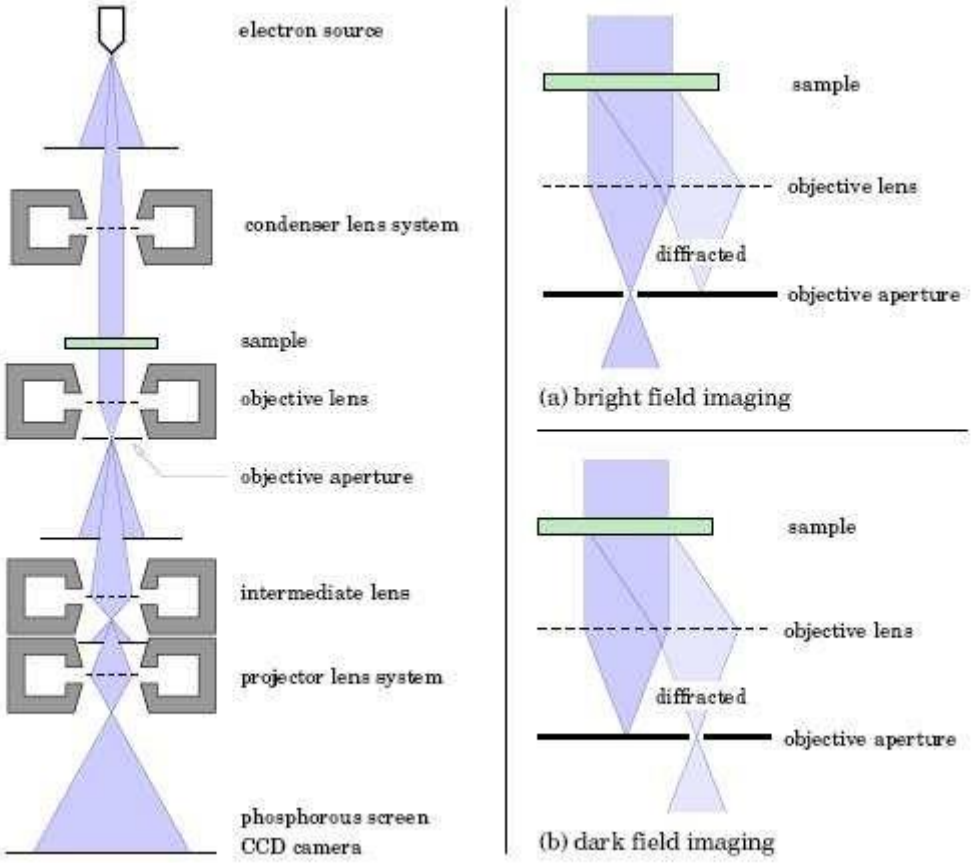

Fig. 18: *Schematic illustration of a transmission electron microscope. The right-hand side shows the two basic imaging modes.*

The two imaging modes seen in fig.13 are the Bright and Dark field imaging. In chapter 4 some pictures of the two imaging modes can be seen. The main difference between the two stands in the manipulation of the electrons. In fact, if the electrons that are not deflected after the transmission in the sample get manipulated with the lenses, then the image would be magnified almost approaching the atomic resolution and giving in turn the so-called bright field image. This means that the brighter regions are the ones with the highest atomic density. If the electrons that are manipulated instead are only the transmitted electrons that

are deviated by a specific angle it would be possible to achieve the opposite of what can be seen from a bright field image, which is the dark field image.

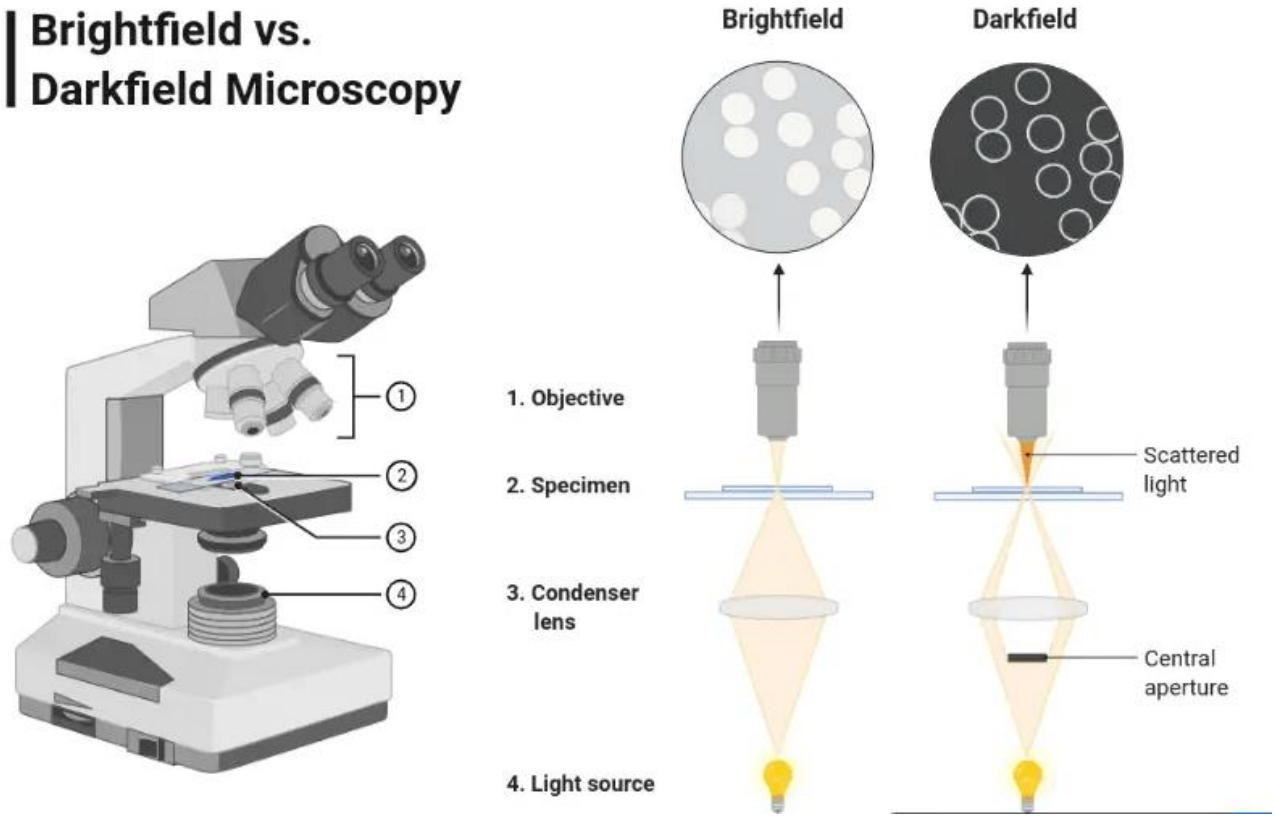

Fig. 19: *Schematic description of the Bright and Dark field imaging.*

In summary, Transmission Electron Microscopes (TEMs) and Scanning Electron Microscopes (SEMs) differ in their imaging mechanisms, sample preparation requirements, and depth of field capabilities. While TEMs provide detailed views of internal structures at the atomic scale, SEMs offer high-resolution imaging of surface topography and composition. Each technique has its strengths and limitations, making them complementary tools for nanoscale imaging and analysis in scientific research and industrial applications.

Chapter 3: Laser Annealing and characterization of the samples

3.1 Introduction

While the first two chapters were mainly focused on giving insight into the nature of SiC, it's amorphous and crystalline phases, its polytypes and the thermal process that leads to the change from the amorphous phase to the crystalline phase, this chapter's aim is to describe the chronological workflow that has been done during the thesis work.
Two different types of lasers have been used, they will both be described later. Before diving deeper, it is necessary to introduce some concepts required to better understand the choice of parameters that will then lead to success or failure in the achievement of the crystallization phase of the amorphous SiC.

3.2 Laser Annealing

The key parameters regarding laser annealing are:

- **Pulse Frequency**: In lasers, the pulse frequency refers to the rate at which pulses of light are emitted. This frequency is typically measured in hertz (Hz), which represents the number of pulses emitted per second. The pulse frequency of lasers can vary widely depending on the specific type of laser, its design, and its intended application. Some lasers operate in continuous wave (CW) mode, emitting a steady stream of light without interruption, so their pulse frequency would be effectively infinite or simply the repetition rate of the energy source driving the laser. However, many lasers are operated in pulsed mode, where they emit light in short bursts or pulses. The pulse frequency in these lasers can range from a few pulses per second to millions or even billions of pulses per second. Ultrafast lasers used for scientific research or industrial applications can have pulse frequencies in the gigahertz (GHz) or even terahertz (THz) range. Controlling the pulse frequency of a laser is crucial for

many applications, as it can impact factors such as precision, efficiency, and the ability to deliver energy in a controlled manner.

- **Scan Speed**: Scan speed in lasers refers to the rate at which a laser beam traverses a surface or volume during a scanning process. This parameter is crucial in various laser applications, including laser engraving, laser cutting, laser scanning microscopy, and laser-based 3D printing. The scan speed is typically measured in units such as millimetres per second (mm/s), meters per second (m/s), or inches per second (in/s), depending on the specific application and the scale of the scan. Optimizing scan speed is essential to achieve efficient and effective laser processing. It involves finding the right balance between speed and quality to meet the specific requirements of the application while maximizing productivity.

- **Power**: Power in lasers refers to the rate at which energy is emitted in the form of light. It is a fundamental characteristic of a laser system and is typically measured in units such as watts (W) or milliwatts (mW), representing the amount of energy delivered per unit of time. This value can be modified up to its maximum value, defined by the laser's chart given by the supplier.

- **Pulse width**: Pulse width in lasers refers to the duration of time over which a pulse of laser light is emitted. It represents the temporal extent of the pulse and is typically measured in units of time, such as seconds, milliseconds, microseconds, or even femtoseconds, depending on the characteristics of the laser and the specific application. The pulse width of a laser pulse is a critical parameter that can significantly influence its interaction with materials and its suitability for various applications. It can affect factors such as the precision of laser machining, the resolution of laser imaging systems, and the depth of penetration in laser-based medical procedures. This parameter represents the watershed between the 532 nm fiber laser and the 355 nm UV laser and a few more words about it will be spent when comparing the twos.

- **Spot diameter**: Spot diameter in lasers refers to the size of the focused laser beam where the intensity of the light is concentrated to a specific region. It represents the diameter of the circular area on the target surface where the laser beam reaches its maximum intensity. It affects both fluence and irradiance.

- **Pulse Energy**: Pulse energy in lasers refers to the amount of energy contained within a single pulse of laser light. It quantifies the total energy delivered by the laser during each pulse and is typically measured in joules (J) or millijoules (mJ), depending on the scale of the energy being considered. Pulse energy is a critical parameter in laser applications, as it directly influences the effectiveness and outcomes of various processes.

- **Fluence**: Also known as energy fluence or laser fluence, refers to the amount of energy delivered per unit area by a laser beam onto a target surface during a single pulse or over a specific period. It quantifies the energy density of the laser's light incident on the target and is typically measured in units such as joules per square centimetres (J/cm^2) or millijoules per square centimetres (mJ/cm^2). Fluence needs to be quite high to allow energy transfer on the material. It strictly depends on power and pulse frequency.

$$Fluence\left[\frac{Joules}{cm^2}\right] = \frac{Laser\ pulse\ energy\ [J]}{Effective\ focal\ spot\ area\ [cm^2]}$$

- **Irradiance**: Irradiance in lasers, also known as optical irradiance or laser irradiance, refers to the power per unit area of a laser beam incident on a surface. It quantifies the intensity of the laser light at a specific point and is typically measured in units such as watts per square meter (W/m^2) or milliwatts per square centimetres (mW/cm^2). This value needs to be quite low, to avoid possible removal of the material. It is related to the pulse width, power, and pulse frequency.

- **Duty Cycle**: The duty cycle in lasers refers to the ratio of the duration of time that a laser is actively emitting light (the "on" time) to the total time of a complete operating cycle, which includes both the "on" and "off" times. It quantifies the percentage of time during which the laser is emitting light versus the total cycle time. The duty cycle is expressed as a percentage.

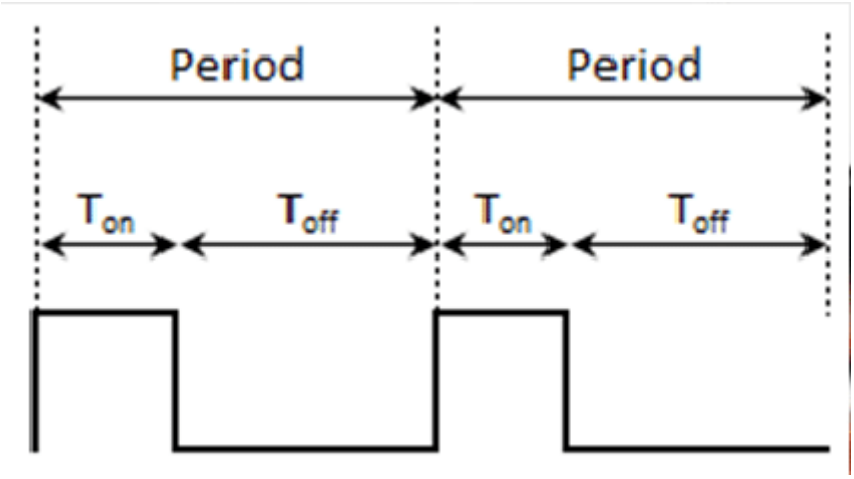

Fig. 20: *Duty cycle diagram.*

- **Peak Power**: Peak power in lasers refers to the maximum instantaneous power achieved during a single pulse or a very short duration of time. It represents the highest intensity of the laser beam and is often a critical parameter in laser applications, especially in pulsed lasers where the power output varies over time. Peak power is distinct from average power, which represents the average power output of the laser over a longer period, typically measured in seconds or minutes. While average power provides information about the overall energy delivery of a laser system, peak power is crucial for understanding the intensity and potential impact of individual laser pulses.

By varying the previously described parameters its possible to finely tune the intensity and so the impact that the laser can have on the samples during the annealing phase, granting both the possibility of achieving the crystallization of the amorphous SiC layer or destroying the sample.

An introduction on the two types of lasers is also required before describing the various tasks that have been completed.

The first chronologically used laser is Vlase model 2109-TFS2 with the following characteristics:

Fig. 21: *Vlase model 2109-TFS2.*

Wavelength	532 nm
Application type	Marking
Emission type	Q-Switched
Observation type	Direct radiation
Pulse energy	Vlase™ 2109-TFS2: 350 µJ @ 20 kHz
Pulse duration	Vlase™ 2109-TFS2: 10 ns
Beam Diameter at 9X Beam Expander Output (1/e2)	Vlase™ 2109-TFS2: 5.0 mm
Beam divergence on the lens	Vlase™ 2109-TFS2: 0.8 mrad
Focal of the F-Theta lens	160 mm
Real divergence after the lens	Vlase™ 2109-TFS2: 31,2 mrad
Exposure time	10 s

Fig. 22: *Parameters of the Vlase model 2109-TFS2.*

The second chronologically used laser instead is the Sol model 4W 355 nm with the following specifications:

Fig. 23: *Image of the Sol UV model 4W 355 nm produced by Bright Solutions.*

Technical Specifications	Typical	
Output Wavelength	355	nm
Output Power	up to 4	W
Pulse Width	15 to 35	ns
Repetition Rate	30 to 100	kHz
Polarization	Linear 100:1	
Beam diameter ($1/e^2$)	< 1 *(option: external beam expander)*	mm
Beam Quality (M^2)	< 1.5 @ 30 kHz	
Electrical Requirements	Dual DC IN 15 V – 12 V (*)	
Cooling	Air Cooled	
Overall dimensions	46 x 17 x 10	cm^3

Fig. 24: *Parameters of the Sol UV model 4W 355 nm.*

The two lasers have in common the emission type, which is Q-switched. Q-switched emission in lasers refers to a technique used to generate short, high-energy pulses of laser light. The term "Q-switched" originates from the method of actively controlling the quality factor (Q-factor) of the laser cavity to efficiently store energy within the gain medium and release it in a short burst.

In a Q-switched laser, the laser cavity includes a Q-switching device, which can be an electro-optic modulator, an acousto-optic modulator, or a saturable absorber. This device temporarily blocks the resonant cavity, preventing the buildup of laser light. The gain medium is pumped to a high energy level, effectively storing energy within the laser system. When the Q-switch is suddenly opened (switched to low-loss mode), the stored energy is rapidly released, resulting in a high-intensity pulse of laser light. This process is known as Q-switching, and it allows for the generation of pulses with extremely high peak powers and short durations.

The key characteristics of Q-switched emission include:

- Short Pulse Duration: Q-switched lasers can produce pulses with durations ranging from picoseconds to nanoseconds. The short pulse duration enables precise control over the interaction of the laser light with materials and minimizes heat-affected zones in laser processing applications.

- High Peak Power: By concentrating the energy stored within the gain medium into a short pulse, Q-switched lasers can achieve very high peak powers. This high peak power is beneficial for applications such as laser ablation, micromachining, and nonlinear optics.

- High Repetition Rate: Q-switched lasers can operate at high repetition rates, allowing for rapid processing of materials and high throughput in industrial applications.

3.3 Specimen Description

Before heading into the description of the annealing treatment and the results obtained right after it, a few words need to be spent on the two different samples that were used during the work thesis:

1. The first sample on which laser annealing has been done can be considered as a test sample to evaluate the efficiency and the quality of the laser annealing process. Graphically, as it can be seen in figure 24, the test specimen is made of 3 specific layers of Si, Silicon dioxide and a-SiC.

Fig. 25: *Graphical description of the Test sample.*

2. The second sample is the main character around which this work of thesis revolves. As for the test sample, a graphic description is required to better recognized the difference with the previous test sample:

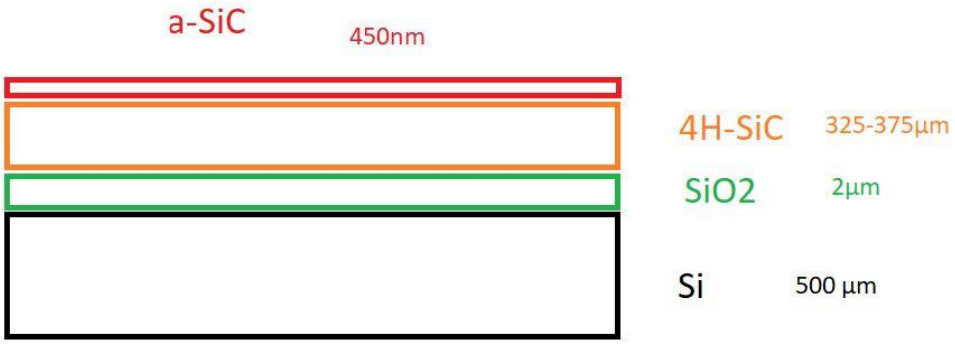

Fig. 26: *Graphical description of the sample used to perform laser annealing for the whole work thesis duration.*

As it can be seen in fig. 27, the structure of the sample is quite like the test sample, except for having an already crystallized layer of 4H-SiC between the SiO2 and a-SiC layer. The layer of 4H-SiC is placed so that it grants a better chance of achieving the crystallization of the amorphous layer during the laser annealing process.

After describing the test specimen and then the actual sample it's possible to describe the obtained results from the laser annealing process that has been carried out on them. Since chronologically the test sample was firstly utilized with the 533nm laser, the following part will describe the obtained results and issues that arose during the work process.

3.4 Specimen's Analysis

The parameters from figure 25 were utilized with the aim of first testing how the test sample would react to the 355 nm laser.

The workflow for the test sample was quite simple and consisted of only two main steps:

1. Laser annealing of the test sample with the Vlase model 2109-TFS2 in vacuum.

2. Analysis of test sample through characterization techniques.

For the test sample the characterization techniques that have been used were Optical Microscopy, X-ray Diffraction Spectroscopy and Raman Spectroscopy. These techniques were already well explained in chapter 2, now the focus will be on what type of information can these techniques deliver.
They will be discussed one by one, going in a chronological order from optical microscopy to X-ray Diffraction and concluding with Raman Spectroscopy.

Optical microscopy was the first characterization technique used; it gives a first glimpse to the sample surface, showing if the annealing treatment has had some effects on the surface of the material or not.

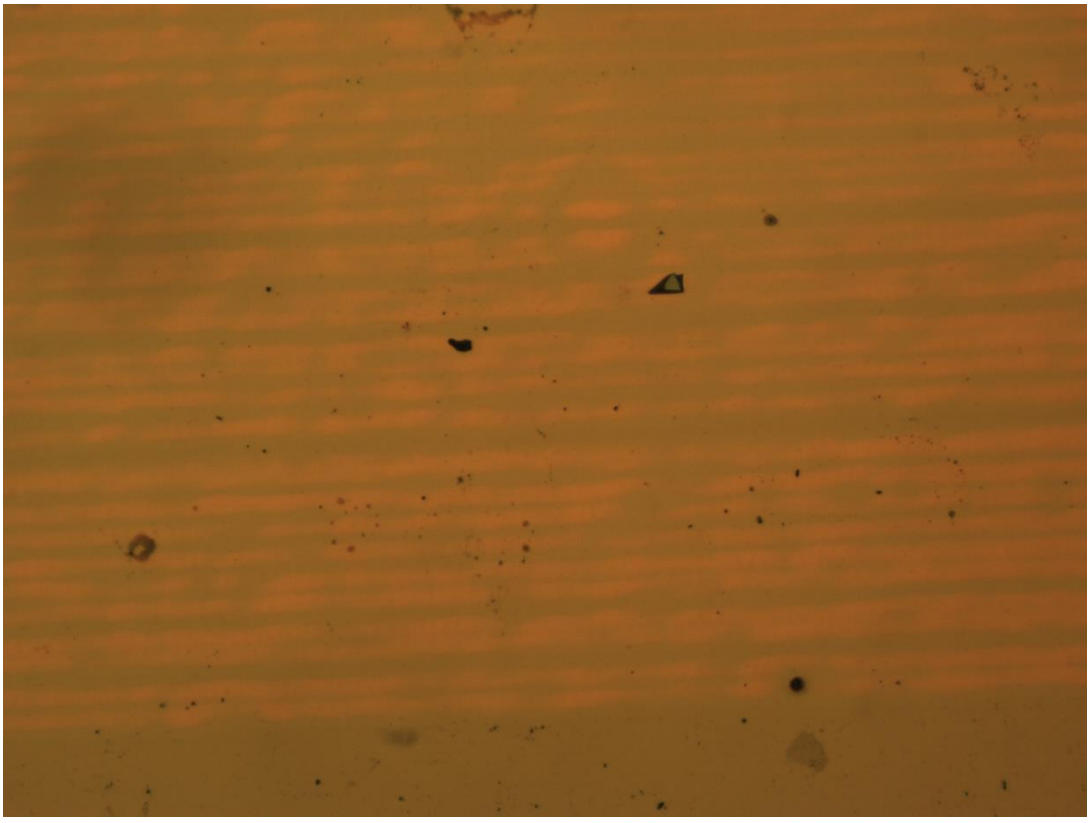

Fig. 27: *Image of the test sample n.12 obtained from a Leica Optical Microscope.*

From the previous figures some conclusions can already be advanced. Figure 28 shows a promising pink colour on top of the sample surface, this could me index of a possible crystallization phase which has happened (even though it's not possible to tell just by using an optical microscope). Figure 29 instead shows a completely different phenomenon. In fact, due to the high energy and extremely low speed parameters that were set into the program guiding the Vlase's laser its possible to see how the topmost layer has been destroyed during the annealing process. This shows how critical the parameter's choice is, since sample 12 had a much lower Power and higher scan speed with respect to sample 18.

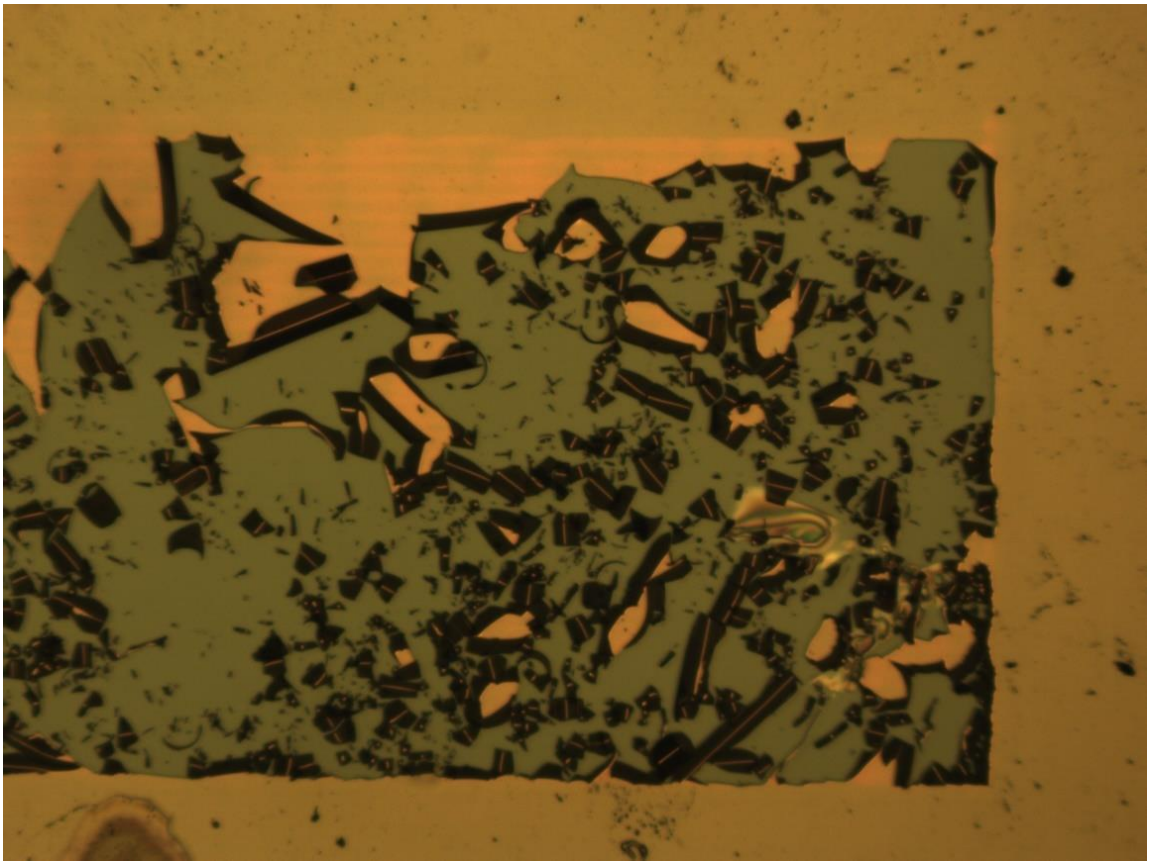

Fig. 28: *Image of the test sample n.18 obtained from a Leica Optical Microscope.*

After inspecting the sample with the Leica's microscope, the next step was to analyse the material composition using another characterization technique, XRD.

X-ray Diffraction analysis on sample 12 and 18 gave the following results:

Spectrum processing:

No peaks omitted.

Processing option: All elements analysed (Normalised)

Number of iterations = 3

Standard:

C CaCO3 1-Jun-1999 12:00 AM

O SiO2 1-Jun-1999 12:00 AM

Si SiO2 1-Jun-1999 12:00 AM

Element	Weight%	Atomic%
C K	34.57	54.83
O K	1.52	1.81
Si K	63.91	43.35
Totals	100.00	

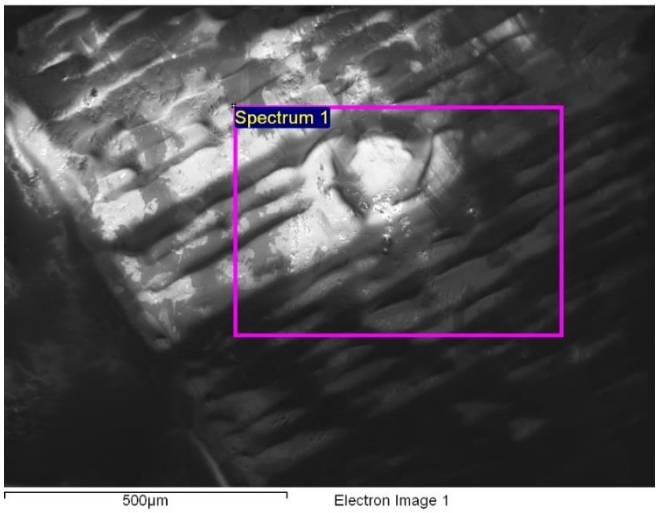

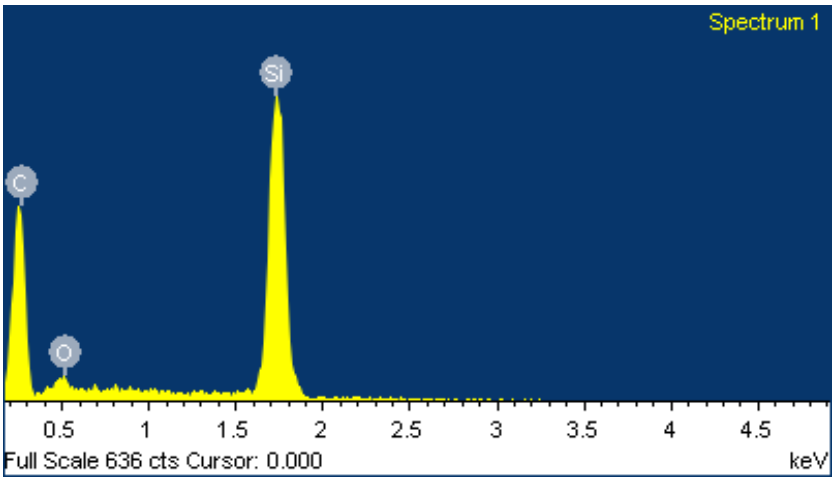

Fig. 29: *XRD analysis of sample 12.*

Spectrum processing:

No peaks omitted.

Processing option: All elements analysed (Normalised)

Number of iterations = 2

Standard:

O SiO2 1-Jun-1999 12:00 AM

Si SiO2 1-Jun-1999 12:00 AM

Element	Weight%	Atomic%
O K	53.13	66.56
Si K	46.87	33.44
Totals	100.00	

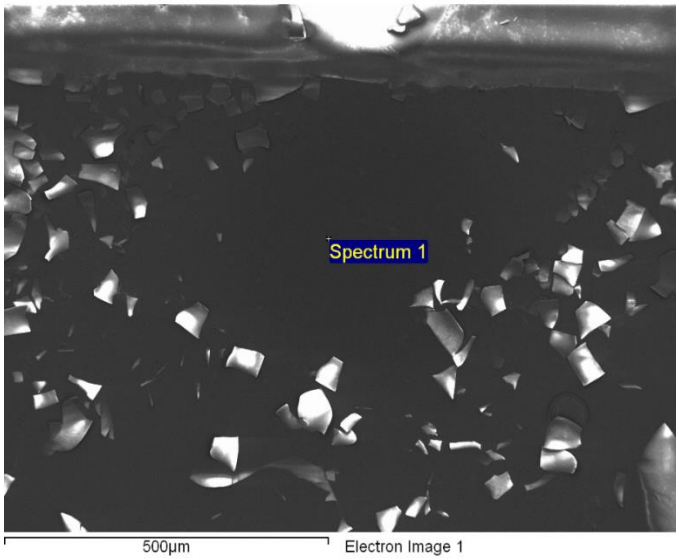

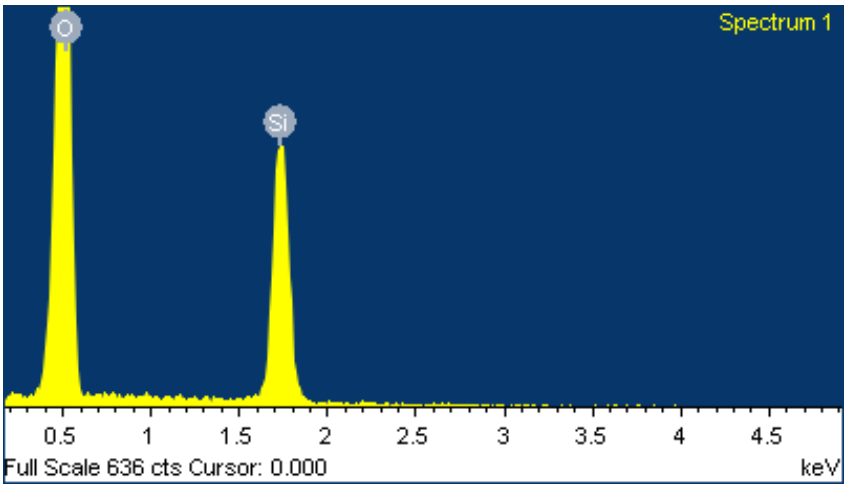

Fig. 30: *XRD analysis of sample 18.*

XRD analysis shows an accurate description of what was previously seen with the optical microscope. In fact, sample 12 presents a well-weighted amount of Si and C respectively, with only a slight amount of Oxygen, meaning that the topmost layer of a-SiC has not been destroyed during the annealing process. In fact, just by taking a glimpse at figure 29 its possible to deduct that sample 18, with the outmost presence of only Oxygen and Silicon, has had its topmost layer of a-SiC completely removed during the annealing process.

The last technique applied to the test sample to obtain information on the possible crystallization phenomenon is Raman Spectroscopy.

Raman Spectroscopy has been the most controversial technique during this work of thesis, and this will be explained much better later. Results obtained with this technique can be seen in the following images:

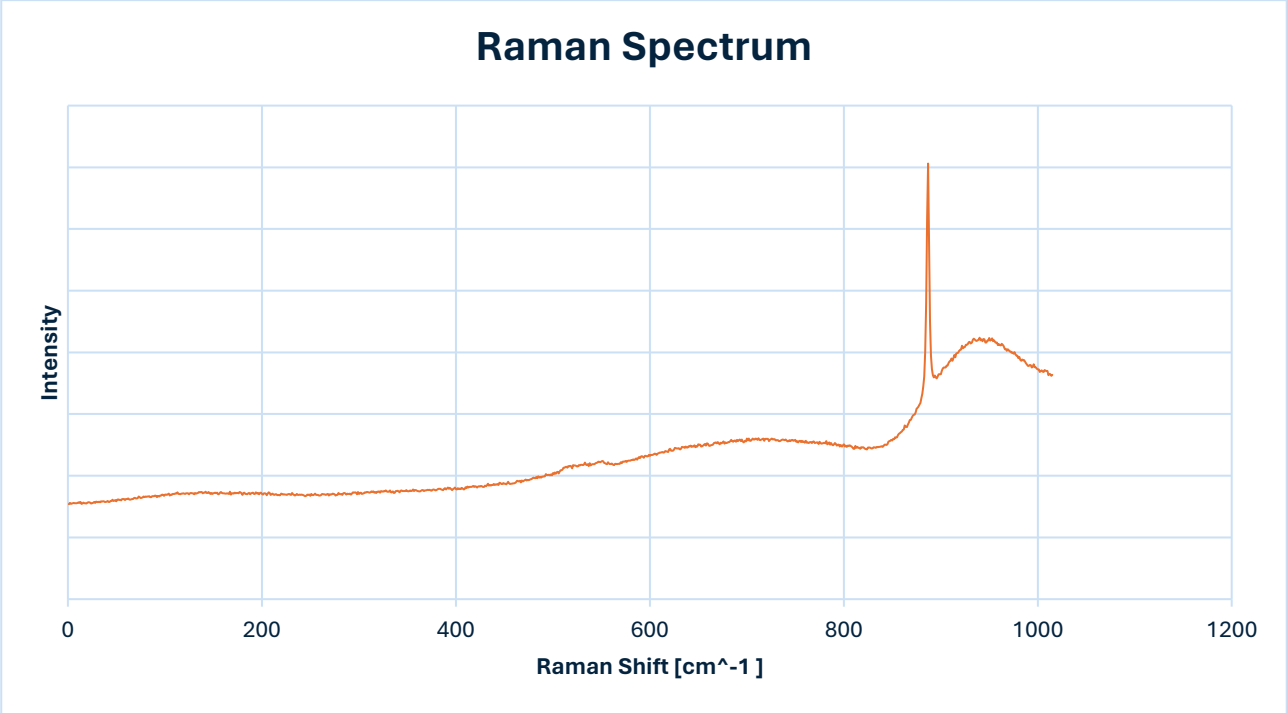

Fig. 31: *Raman Spectrum of sample 12.*

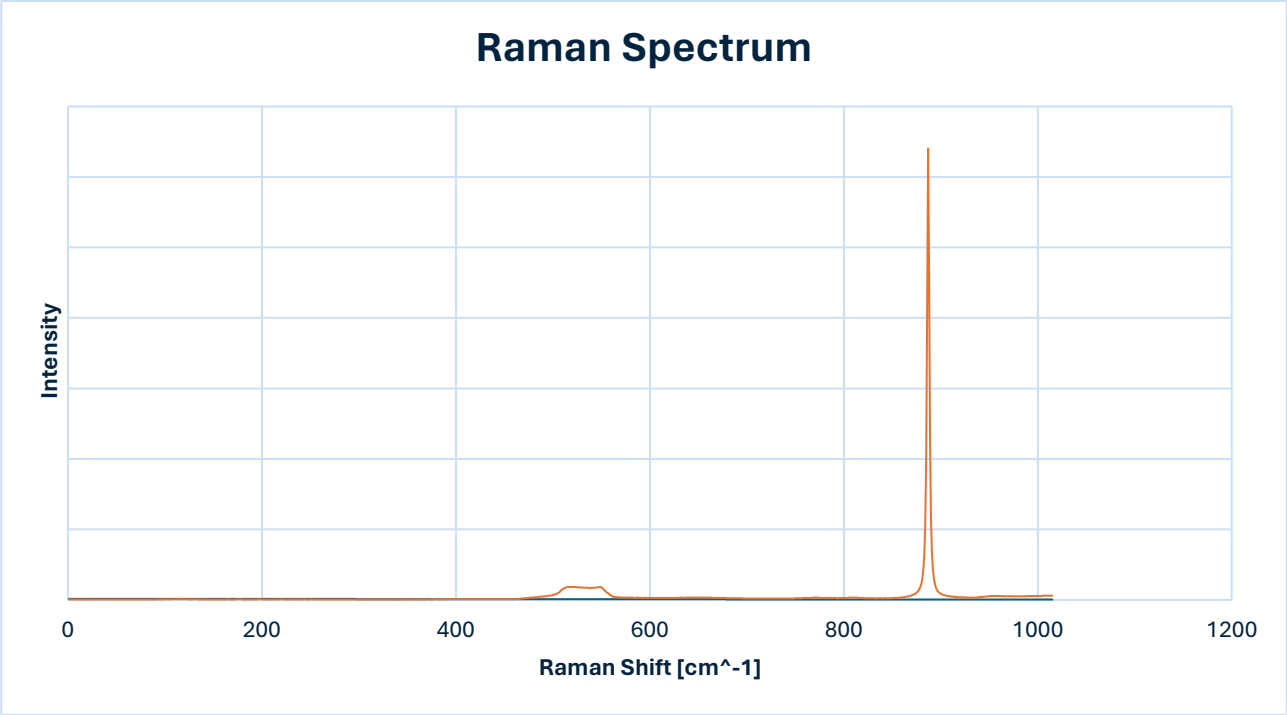

Fig. 32: *Raman Spectrum of sample 18.*

As it was seen in chapter 2, we should find, at least for sample 12, a peak around 780 cm^-1, where SiC shows crystallinity. This does not happen and in fact, by looking at figure 32 it's easy to see that there are no peaks around that Raman shift's value while the small bump at around 500 cm^-1 is related to Si. The same thing goes for figure 33, even though just from the XRD image we were almost certain about the fact that no crystallographic behaviour could be seen.

The Fiber laser clearly shows limits regarding the possibility of crystallizing the topmost layer composed of amorphous Silicon of the test sample. So, the question should be, why is the second UV laser better? What does it change with respect to the 533 nm laser?

The answer is the pulse width. The 533 nm laser cannot in any way change its pulse width value which results to be fixed to 10 ns. The UV laser instead presents a wide range of values going from 10 ns up to 35 ns. It's clear how this can be advantageous since the pulse width of a laser pulse is a critical parameter that directly and significantly affects its interaction with the material.

From this point on in the chapter, we will only consider the UV laser, leaving behind the not so useful green laser. One more remark needs to be made on the sample material; in fact, the test sample composed of Si-SiO2-aSiC will not be used anymore and permanently replaced by the definitive specimen that was previously described.
This time, a setup was built around the idea of performing laser annealing in a vacuum environment so that by removing oxygen, issues like surface contamination, oxidation, material damage or simply annealing efficiency reduction can be avoided. To do so, the specimen was placed into a small cavity that would then be mechanically closed by placing on top of it the magnification lens that would take the role of focusing the laser beam; this cavity would then be connected to vacuum pump which will be turned on and off every time, performing a new annealing process on a new sample.
Another important remark needs to be given to the lens previously mentioned. A cleaning process, achieved by injecting nitrogen into the closed chamber, will ensure that no contamination or residues will be left on the surface of the lens which could lead to a

decrease in the efficiency of the annealing process. To sum up the steps in chronological order are:

1. Opening of the chamber and positioning of the sample.
2. Cleaning process by injecting nitrogen inside the chamber.
3. Turning the vacuum pump on and waiting a few minutes until the pressure monitored by the program is reduced to a few millibars.
4. Laser annealing process.
5. Turning off the vacuum pump and taking the sample out of the chamber, ready to be analysed.

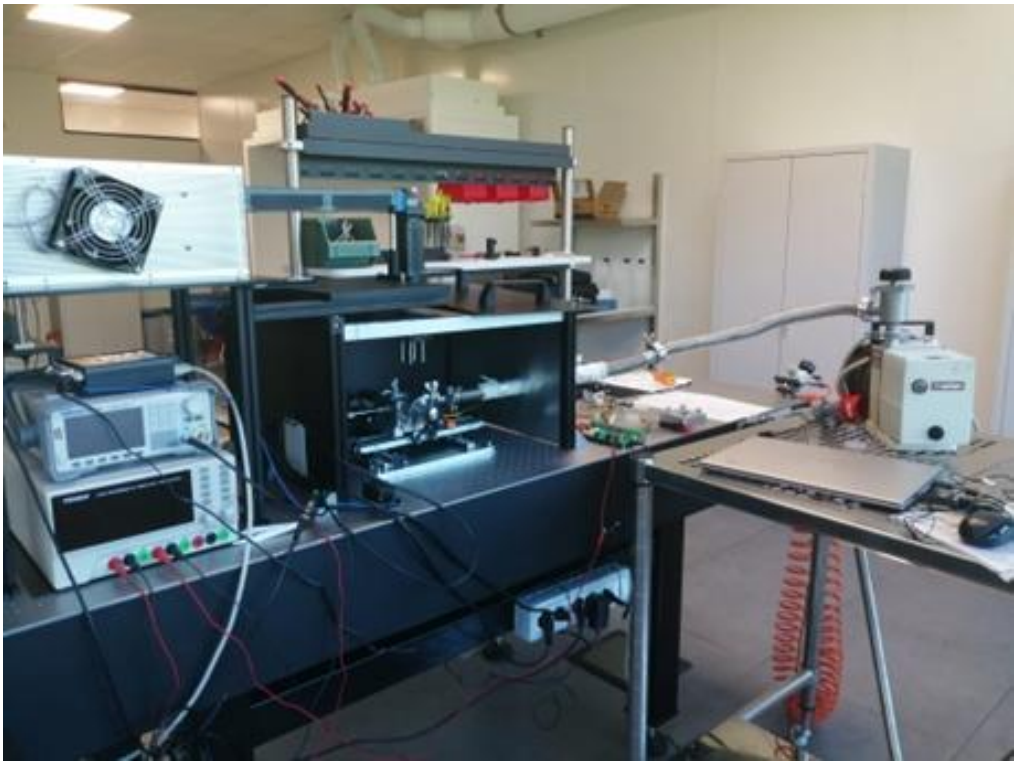

Fig. 33: *Image of the setup built to perform laser annealing.*

Following the steps previously described more than 40 samples have been annealed by varying the parameters that were described at the beginning of the chapter and that can be seen in fig. 35.

	10%	20%	30%	40%	50%	60%	70%	80%
30 kHz	0,06	0,25	0,55	0,95	1,39	1,84	2,37	2,97
40 kHz	0,05	0,18	0,41	0,74	1,12	1,58	2,03	2,5
50 kHz	0,04	0,14	0,33	0,59	0,93	1,3	1,75	2,2
60kHz	0,04	0,12	0,27	0,5	0,77	1,12	1,48	1,95
70kHz	0,04	0,1	0,23	0,42	0,66	0,95	1,3	1,66
80kHz	0,03	0,09	0,2	0,36	0,58	0,84	1,16	1,47
90kHz	0,03	0,08	0,18	0,32	0,5	0,74	1,04	1,38
100kHz	0,03	0,08	0,16	0,28	0,47	0,65	0,92	1,37

Fig. 34: *Table containing all the parameters used to perform laser annealing on the sample.*

The previous image shows the average power value (green), obtained by selecting the Pulse frequency (values on the left in kHz) and Duty Cycle (values in percentage on top) values. The initial selection of values was at first done randomly, since not much information was accessible from the point of how much these parameters influence the laser annealing process. In fact, by taking a first look at the first samples that were done it's easy to see how either the pulse frequency or the duty cycle values were too high at first, removing completely the topmost layer of the specimen.

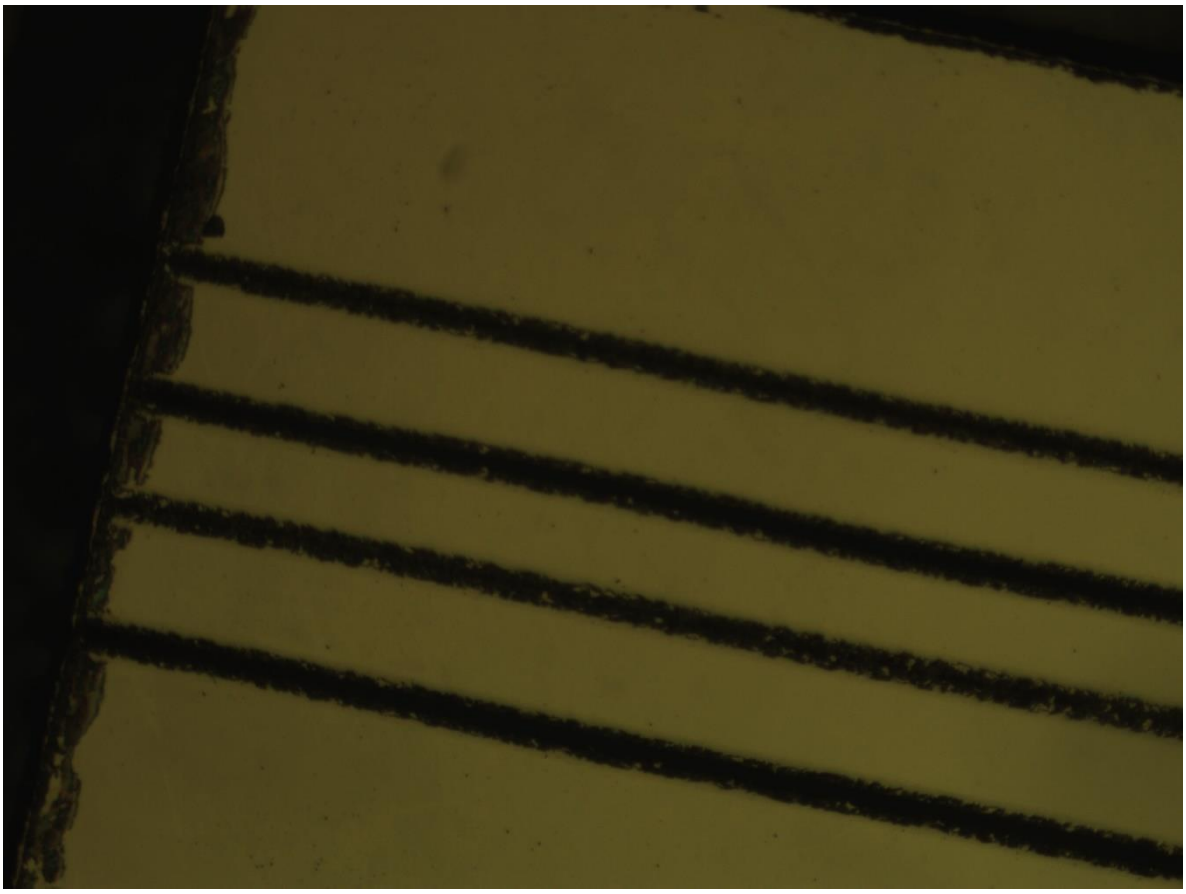

Fig. 35: *Image showing one of the first annealed samples with different parameters of frequency and duty cycle.*

This process of selecting the suitable parameters regarding frequency, duty cycle and scanning speed could be described initially as a trial-and-error task in the beginning but, after annealing more samples and observing the behaviour of the various parameters, that were changed after every annealing, a thinning of the possible combinations of values for frequency and duty cycle can be done. What pops out is that the most promising values which could grant a possible crystallization of the amorphous layer of SiC are the ones were the average power value floats between 0.66 and 1.2 W. This means that samples that are laser annealed with values of pulse frequency between 60-70 kHz and Duty Cycle percentages between 50-70 % could indeed give us good results.

A good example of what has been previously stated is the choice of the two next lines (shown in figure 3), that will be studied in chapter 4 with TEM characterization technique.

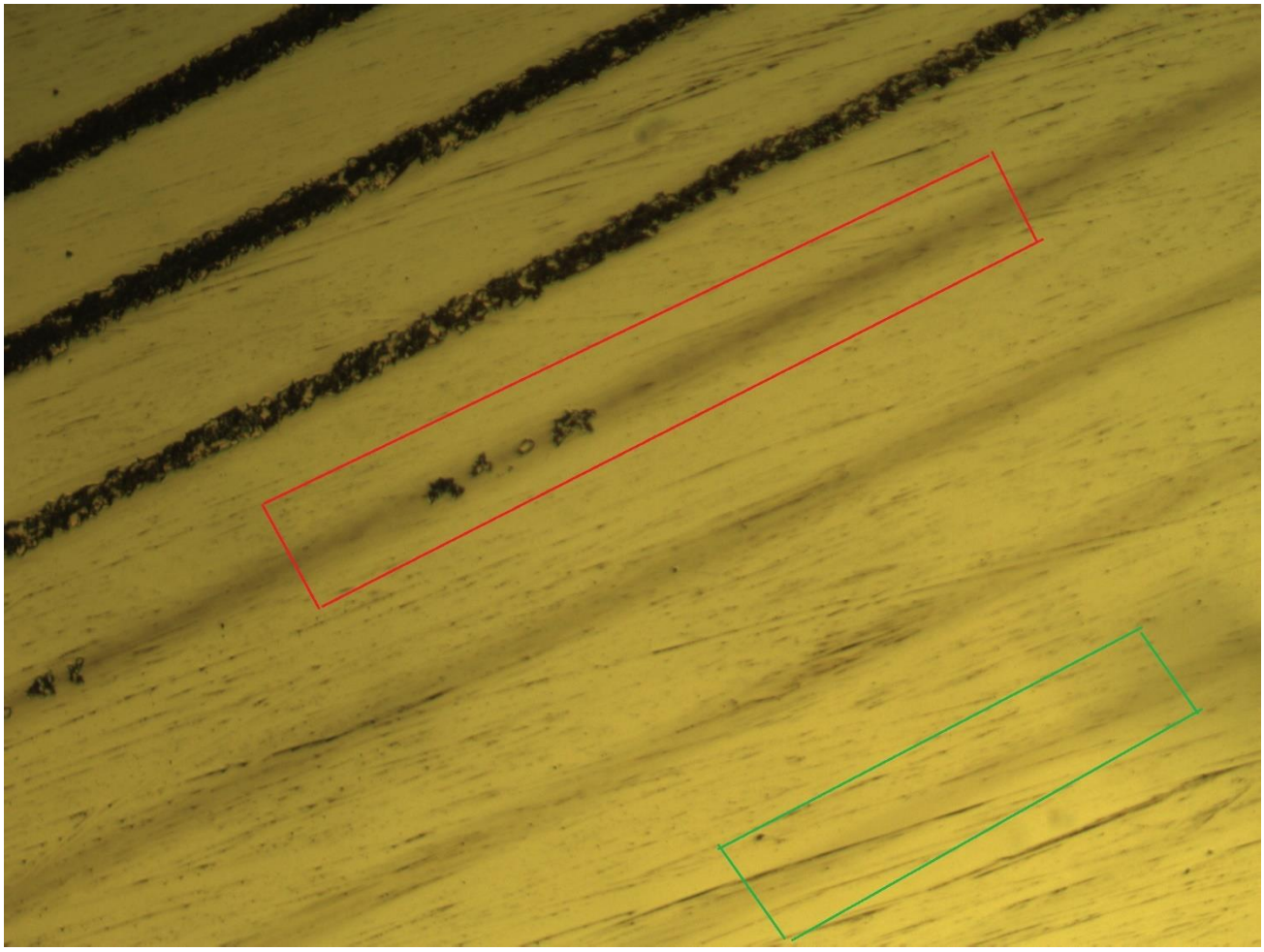

Fig. 36: *Line 4 and 7, chosen from the sample group G.*

The chosen lines that will be analysed in the next chapter are the fourth (red) and the seventh one (green), both coming from the laser annealed sample of group G. To obtain a clear view of what the results could be like, these two were picked. In fact, the red one is the most visible but not burnt by the annealing process while the green one presents the weakest visible line between all the others.

Full focus on the preparation and analysis of these two lines will be given in the next chapter; to conclude this section instead, a quick remark needs to be done on the unavailability of achieving Raman Spectroscopy on this sample, which differs from the previous one (on which we were able to perform Raman spectroscopy, even though results were quite poor).

But why Raman doesn't work on the new sample?

The issue with Raman spectroscopy arose when we tried to perform an analysis on one of the first annealed sample.

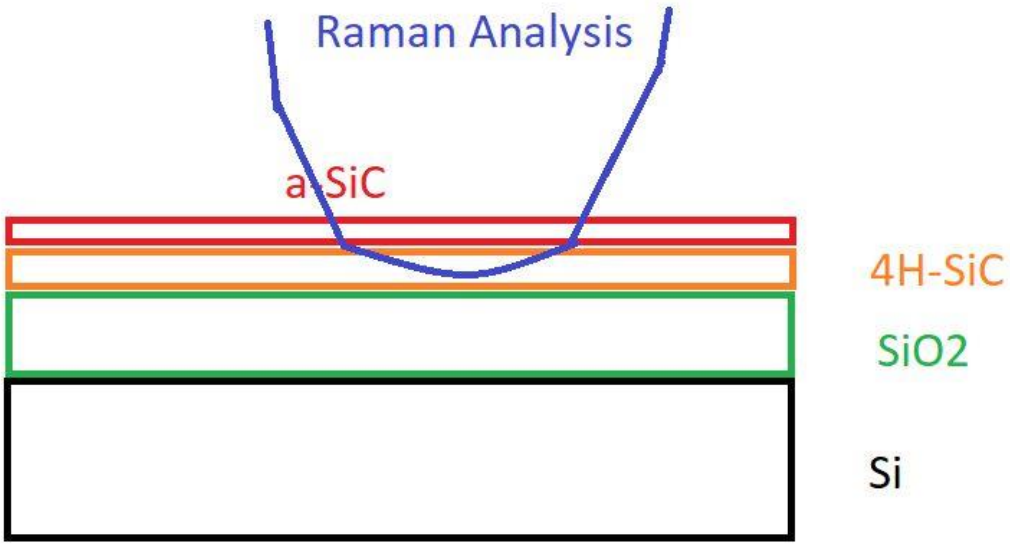

Fig. 37: *Image showing the Raman's Area in which the analysis of the sample takes place.*

Fig.38 shows in blue the average Area where the Raman Spectroscopy analysis takes place. The dire issue with this technique is that, if the red layer of a-SiC would crystallize through the laser annealing process, it would not be recognizable with respect to the subsequent layer of 4H-SiC which is already crystalline.

One good answer could be to move the focusing distance so that the blue area could only analyse the a-SiC layer, without taking into account the contribution on the spectrum of the 4H-SiC layer, but since a change in the blue area where the analysis takes place can only be done by moving the focus position, which is fixed to values of 5, 10,15 and 20 µm, this leads to the problem of going out of focus if the chosen value is for example 25 µm.

One Raman analysis has been done by setting the focusing distance at 25 µm and the obtained spectrum would completely loose the contribution at 780 cm^-1 previously

described, while instead, by analysing at 15 or 20 μm, the spectrum would show the crystal behaviour of 4H-SiC, even though the a-SiC layer hadn't undergone the laser annealing process.

This leads to a discard of the Raman Spectroscopy technique as a characterization technique for our sample, leading to the introduction of the Transmission Electron Microscopy technique, as shown in the next chapter.

Chapter 4: Lamella preparation and Transmission Electron Microscopy Analysis

4.1 Introduction

This chapter will focus on the preparation of the sample with the Focused Ion Beam and then discuss the characterization of the obtained thin lamella with the Transmission Electron Microscopy.

A brief introduction of the Focused Ion Beam technique is required to better understand the upcoming process.

4.2 Focused Ion Beam and lamella preparation process

Principles of operation of FIB and SEM are conceptually identical. At the top of the electron optical columns there is a source of charged particles, ions for the FIB and electrons for the SEM.

Fig. 38: *SEM apparatus with the FIB column added on the left.*

As it can be seen in the previous figure, the FIB column is an addiction to the SEM setup that was already described in chapter 2. In fact, the FIB preparation of the lamella, which consists of various steps that will be described in a moment, is done thanks to the possibility of working with the Dual Beam configuration.

The dual beam configuration simply consists of using the FIM for the ablation part while the SEM keeps track of what is happening on the surface of the sample in real time. FIB can be also used for scanning, just like the SEM but typically it is only used once before starting the etching process, just to achieve a better focus of the sample part that needs to be etched.

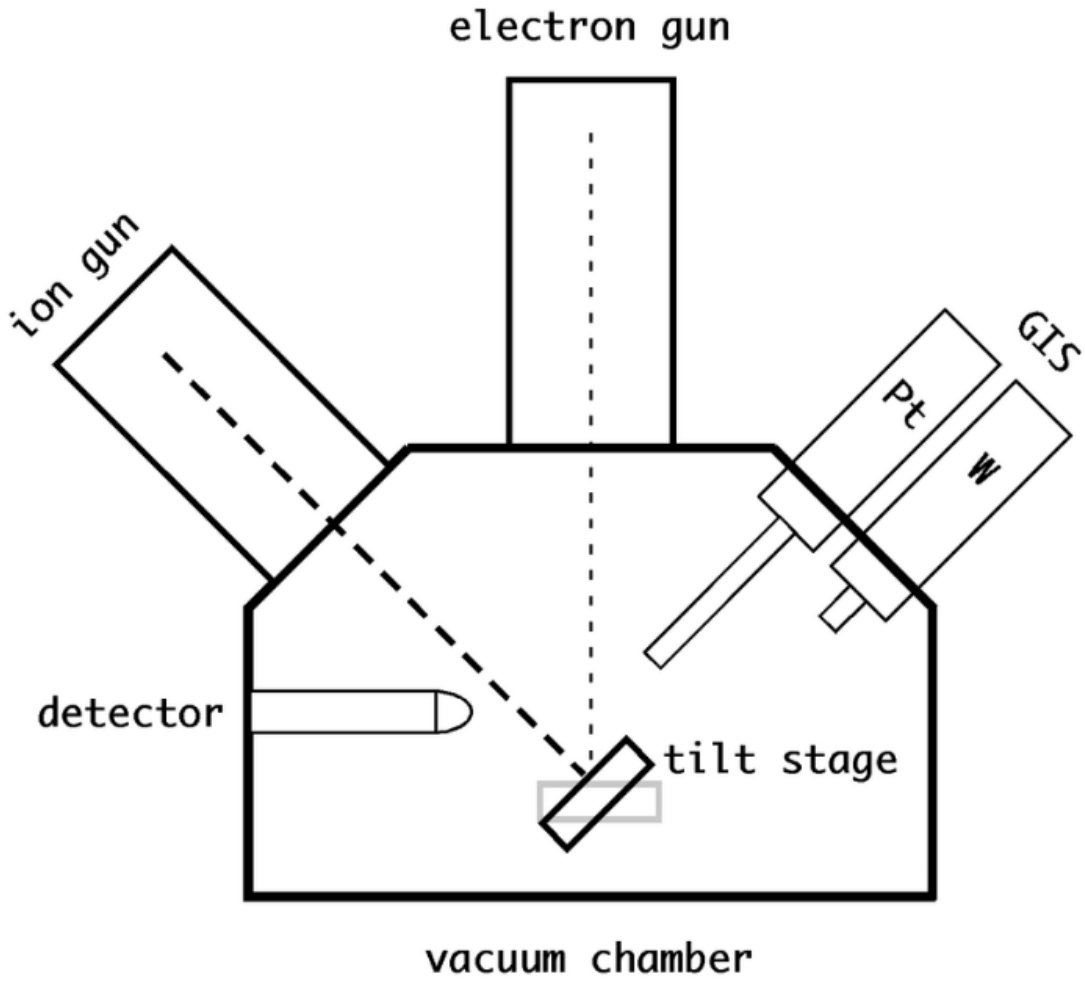

Fig. 39: *Dual Beam Configuration.*

Let us start now with the description of the various steps needed to obtain the lamella from the full sample:

1. **Metallization**: A 20 nm platinum layer is deposited at the site of interest by sputtering process.

2. **Protective Layer**: Subsequently a 2µm protective layer of platinum is deposited. This is done by decomposition of an organic molecule (Trimethyl platinum) that has been injected into the chamber, close to the surface, which favours the release and consequently deposition of platinum when the ionic beam hits it.

3. **SEM and FIM preliminary scan**: The FIB and SEM energies are set respectively at 30Kev and 5Kev. The FIB will only be used to align the portion of the sample that needs to be etched while the SEM will be used to achieve a real time imaging (even though the image is refreshed every 30 seconds). In this configuration, SEM uses secondary electrons. This is quite important since the detector is quite sensitive to the derivates of the sputtering caused by the ionic beam.

4. **Front Stairs**: The FIB utilizes Xenon ions, which are heavier than the more commonly used gallium atoms; this grants a higher etching speed while keeping the energy of the beam still. Also, since Xenon is a noble gas there will be no risks regarding the possible creation of an alloy (this can happen with gallium ions instead). Finally, one more advantage of utilizing Xenon ions is that they allow the usage of higher currents for excavations, starting from nanoamperes up to few picoamperes. The result of this part can be seen in the following figure: this first ion beam etching is done by tilting the sample at 55 degrees so that its surface can be looked out to the ionic column and two cross sections are cut from both sides towards the protective strip.

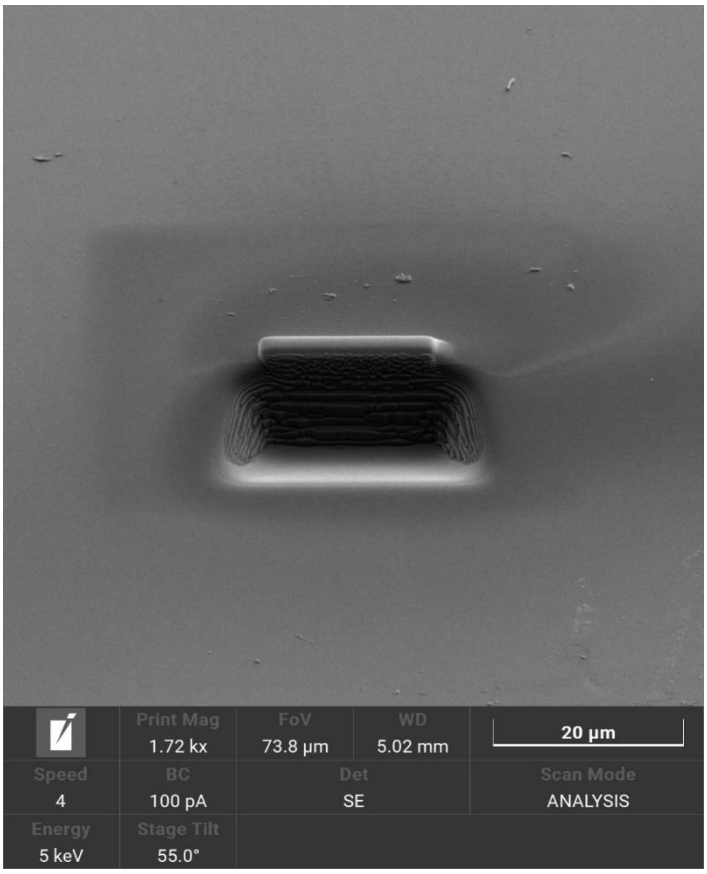

Fig. 40: *SEM image of the first etched side.*

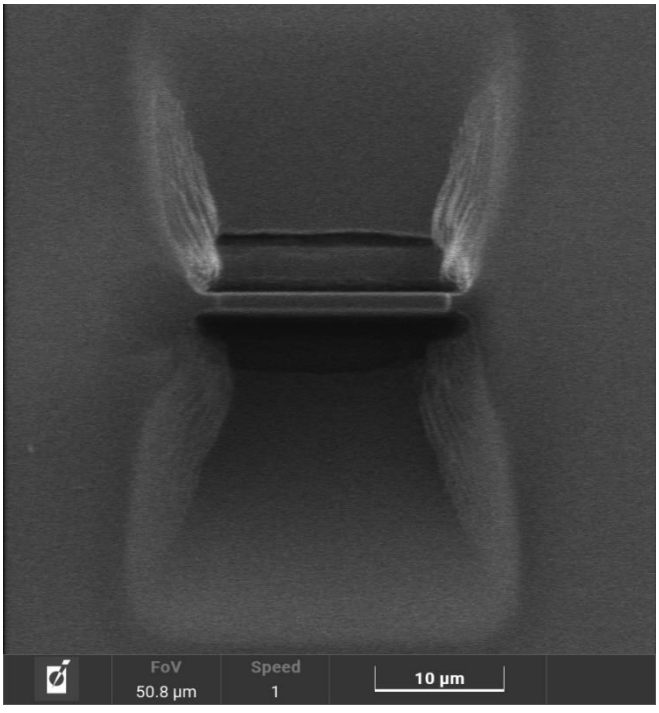

Fig. 41: *FIB image of both the etched side.*

5. **SEM check**: A SEM scan is required to check the obtained excavations.

6. **Front Polish**: To get the typical rectangular shape, we further tilted the sample, reaching 57.5 degrees and then used the ion beam to achieve a fine polish of 1-1.5 µm on both sides. Since this step will be the major contributor to realize a precise rectangular structure, a lower current of around 1 nanoampere was used.

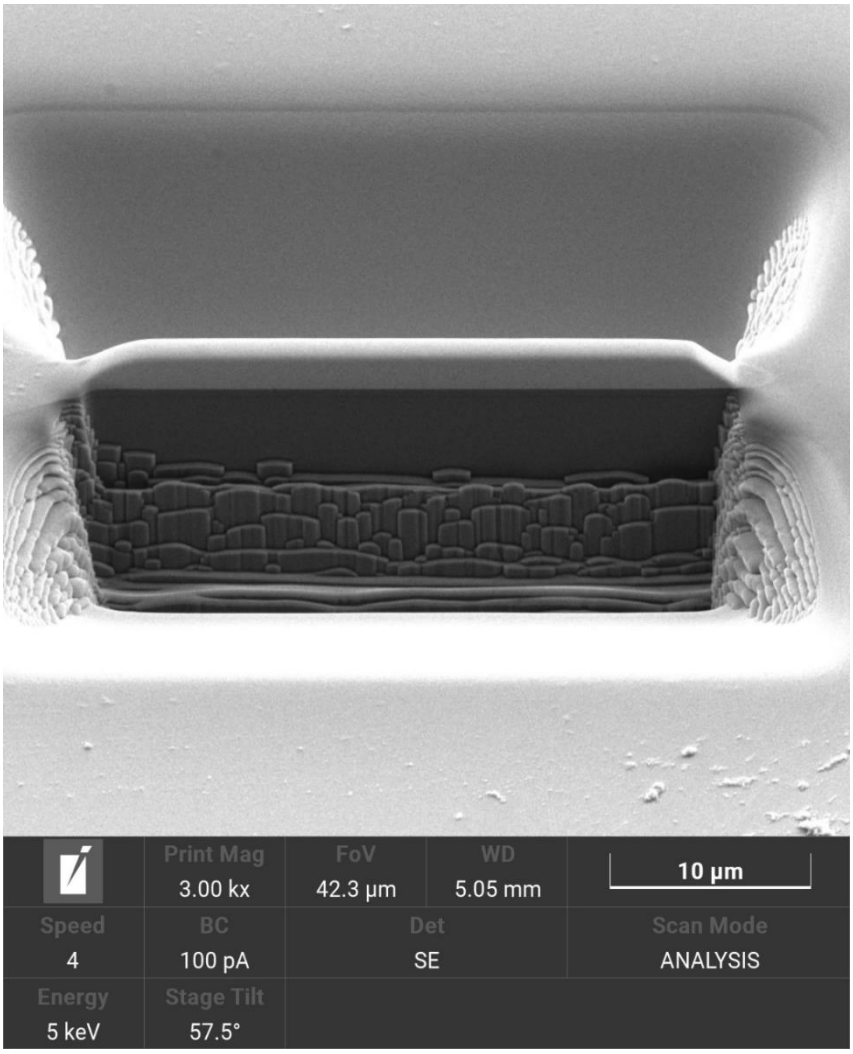

Fig. 42: *SEM image of the front polish step.*

7. **Positioning of the Grid**: Before carrying out the J-cut the program that is running the various steps requires to save the position of the clamp on which a grid will be positioned. The physical position is then saved, ready to be used in the next steps.

8. **J-cut**: This is the most crucial part of the entire preparation process. Physically, a lateral cut (with respect to the lamella position) needs to be made; since the precision and sensitivity of the ion beam needs to be quite high, we reduced the current to a few nanoamperes. This process is quite time consuming and a continuous monitoring with the SEM scanning is indeed required to keep track of which portion of the sample the ion column is etching. The result will be a lamella that is still attached to the sample. One important aspect of this face is how the SiC showed to be a tough material to be etched due to its high hardness. A consequence of what was previously said is the need of increasing the tilting angle at 58.5 degrees.

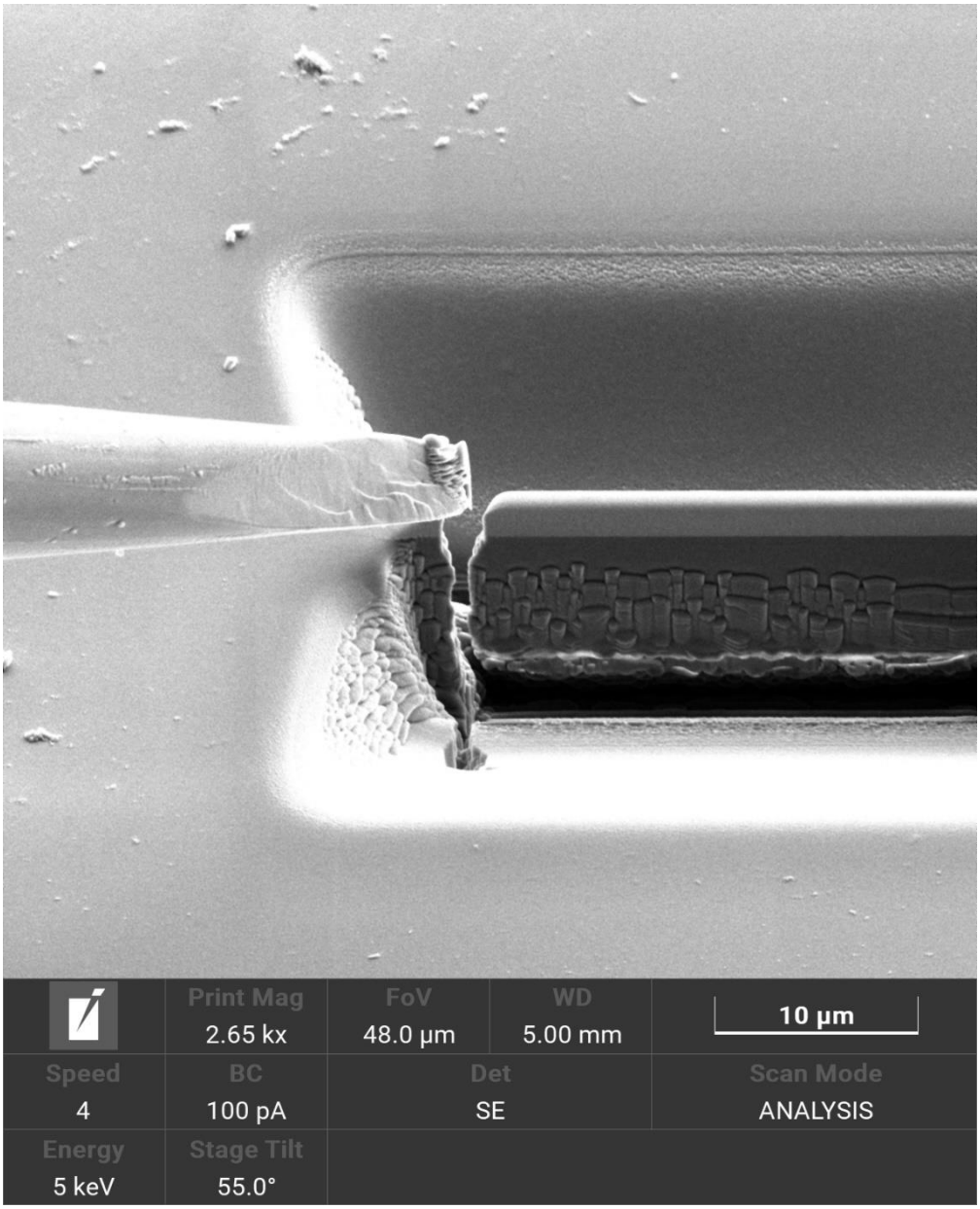

Fig. 43: *SEM image of the achieved J cut and enclosing of the tip.*

9. **Attaching of the tip to the lamella**: Once the J-cut has been done a manipulator is introduced inside the chamber. In this phase, the nail needs to be moved through an independent mechanical system of piezoelectric nature and always monitored with the real time SEM scanning. Mechanical speed can vary from 1 to 10 µm/s. The two elements need to be well placed, almost touching each other.

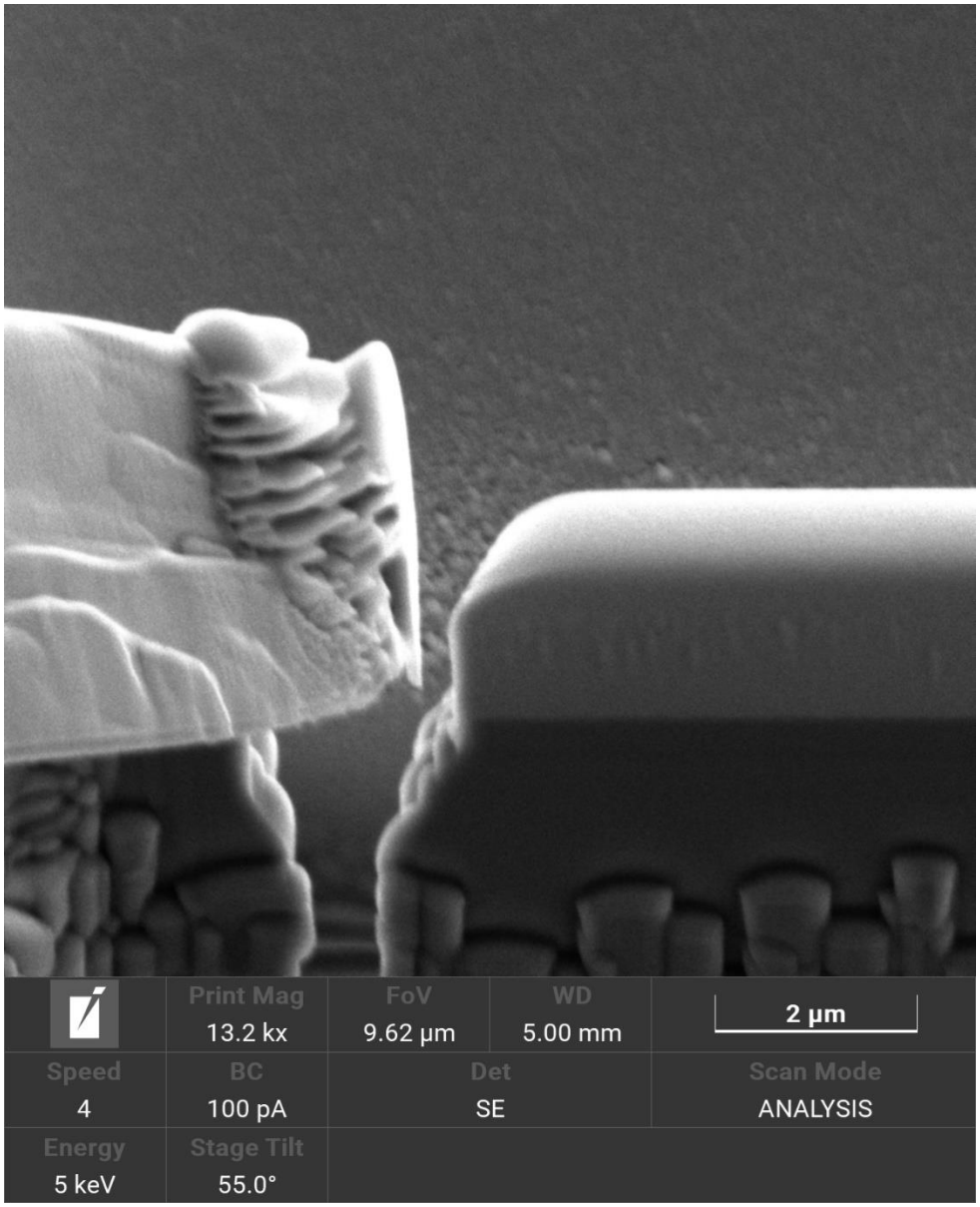

Fig. 44: *SEM image of the tip approaching the lamella.*

10. **Welding Tip-Lamella**: This process lasts one minute and is necessary to grant the effective attachment between the tip and the lamella. This is achieved by injecting into the chamber the same precursor gas utilized for step 2 and employ the ion beam to allow the deposition of platinum in such a way to create a bridge between the tip and the lamella. A nice remark that needs to be remembered here is that for nonconductive samples there may be electrostatic interactions (primarily repulsion here) between charges that can generate a rupture with the tip of the nail, leading to a loss of the lamella.

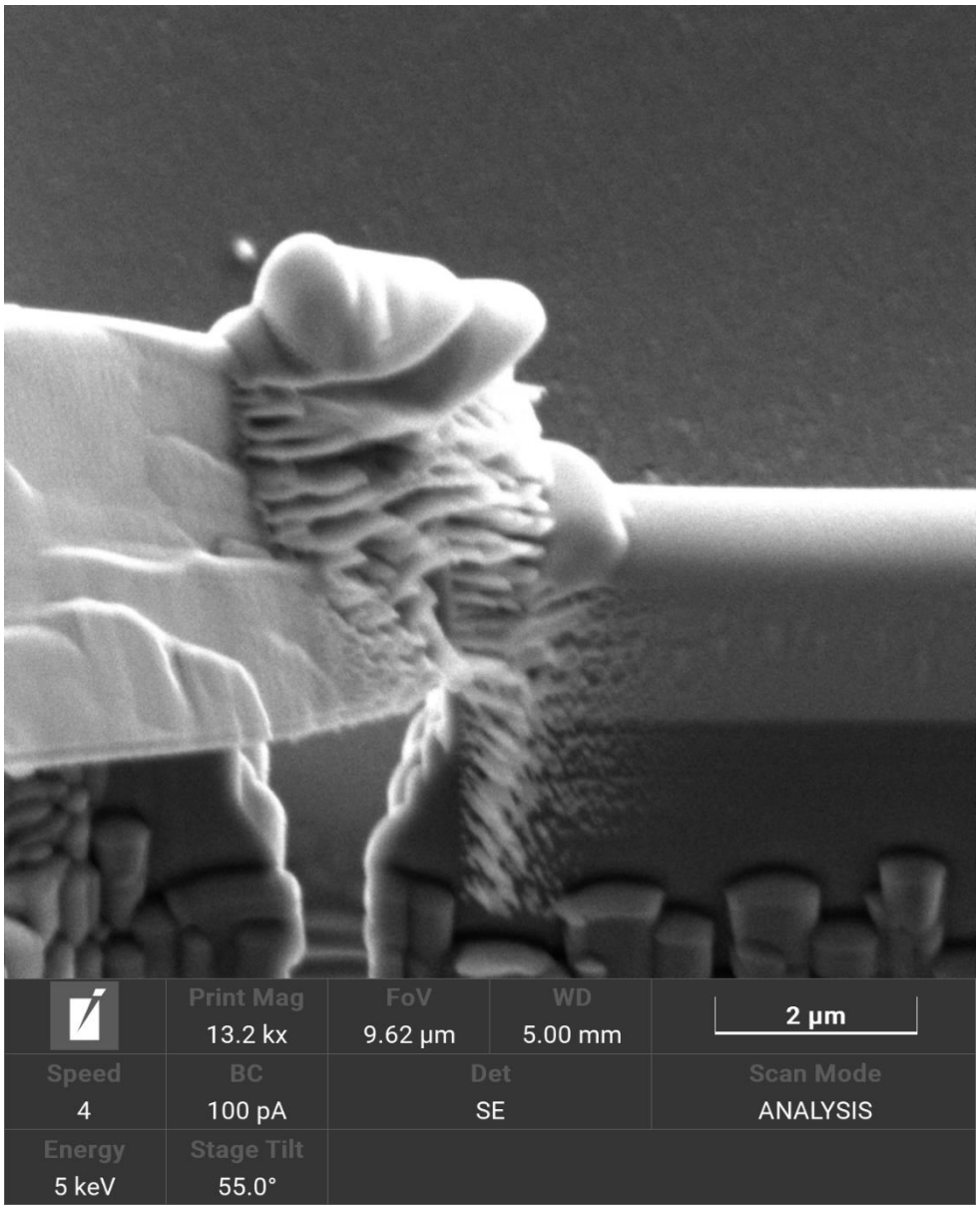

Fig. 45: *SEM image of welding between the tip and the lamella.*

11. **Lamella Cut out**: The lamella, through an etching phase, is finally cut out. In this phase the cutting speed its quite high and the currents utilized are of the order of 250 picoampere.

Once the cut out is done the stage is moved to control if the weld between the lamella and the tip has been completed. After this check a recall of the saved position of the grid, previously described in step 7, is done and the lamella is moved close to the grid.

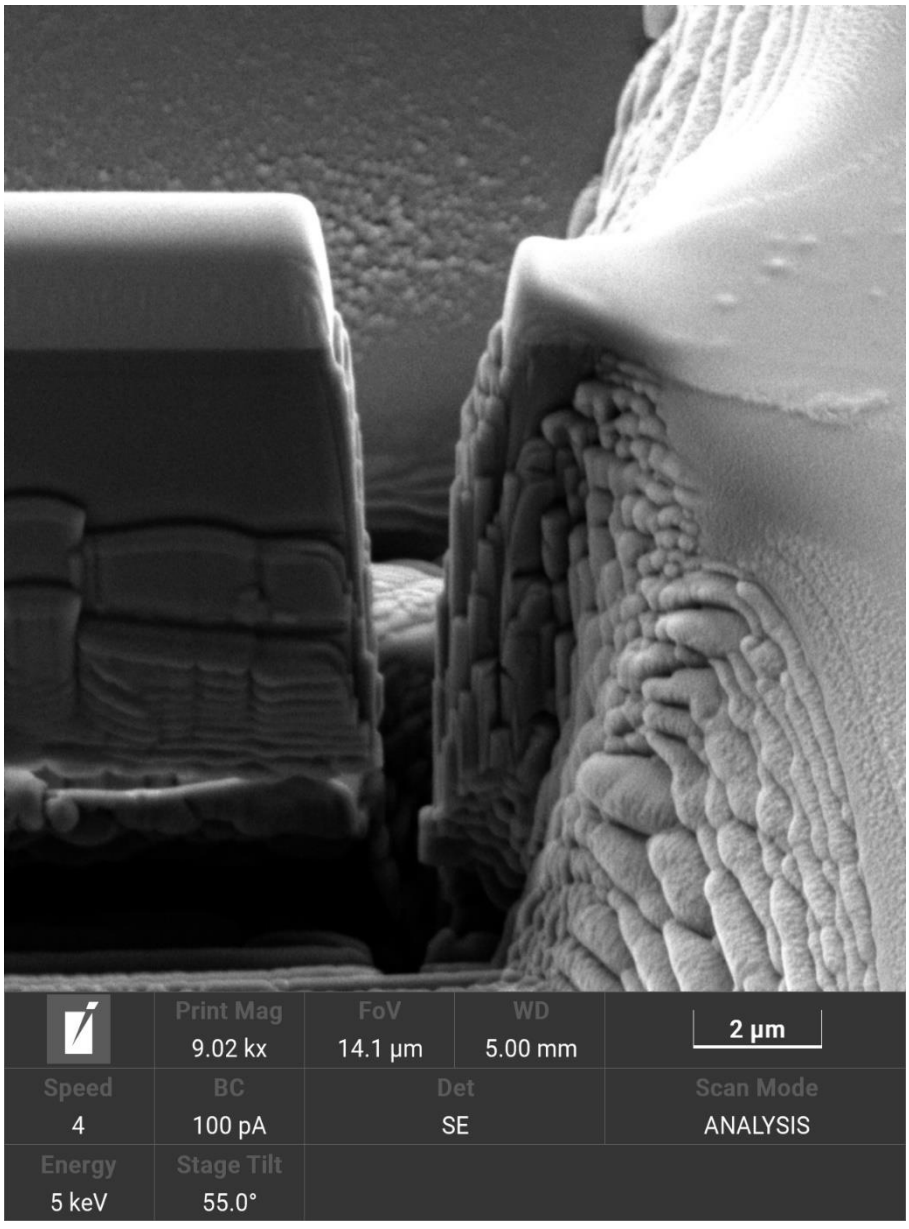

Fig. 46: *SEM image of the lamella's cut out.*

12. **Attaching of the Lamella to the grid**: This conclusive step is done thanks to the introduction of a second nanomanipulator which boosts extreme precision and sensitivity. Once the lamella is close enough to the grid another welding process is required which will anchor the lamella to the grid, ready to be analysed with the TEM.

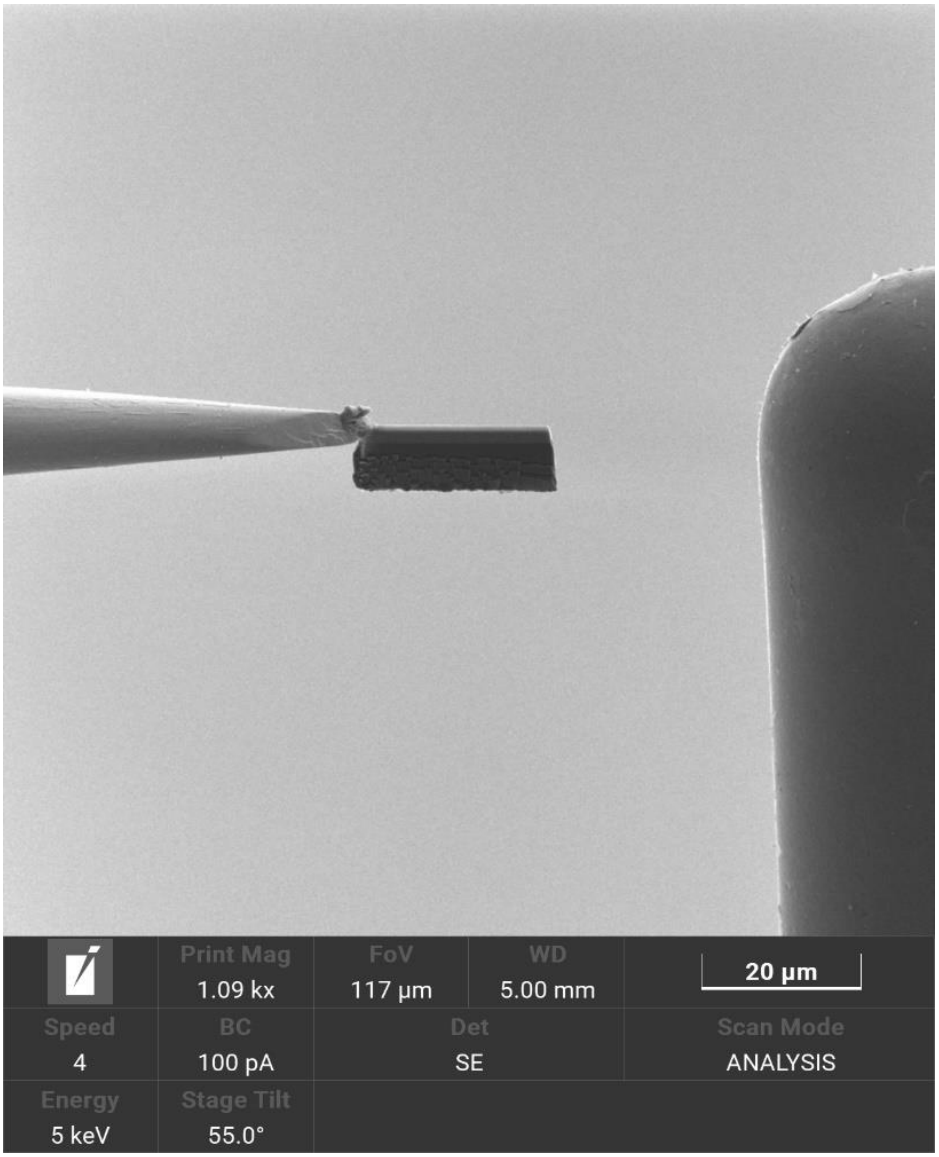

Fig. 47: *SEM image of the positioning of the lamella close to the grid.*

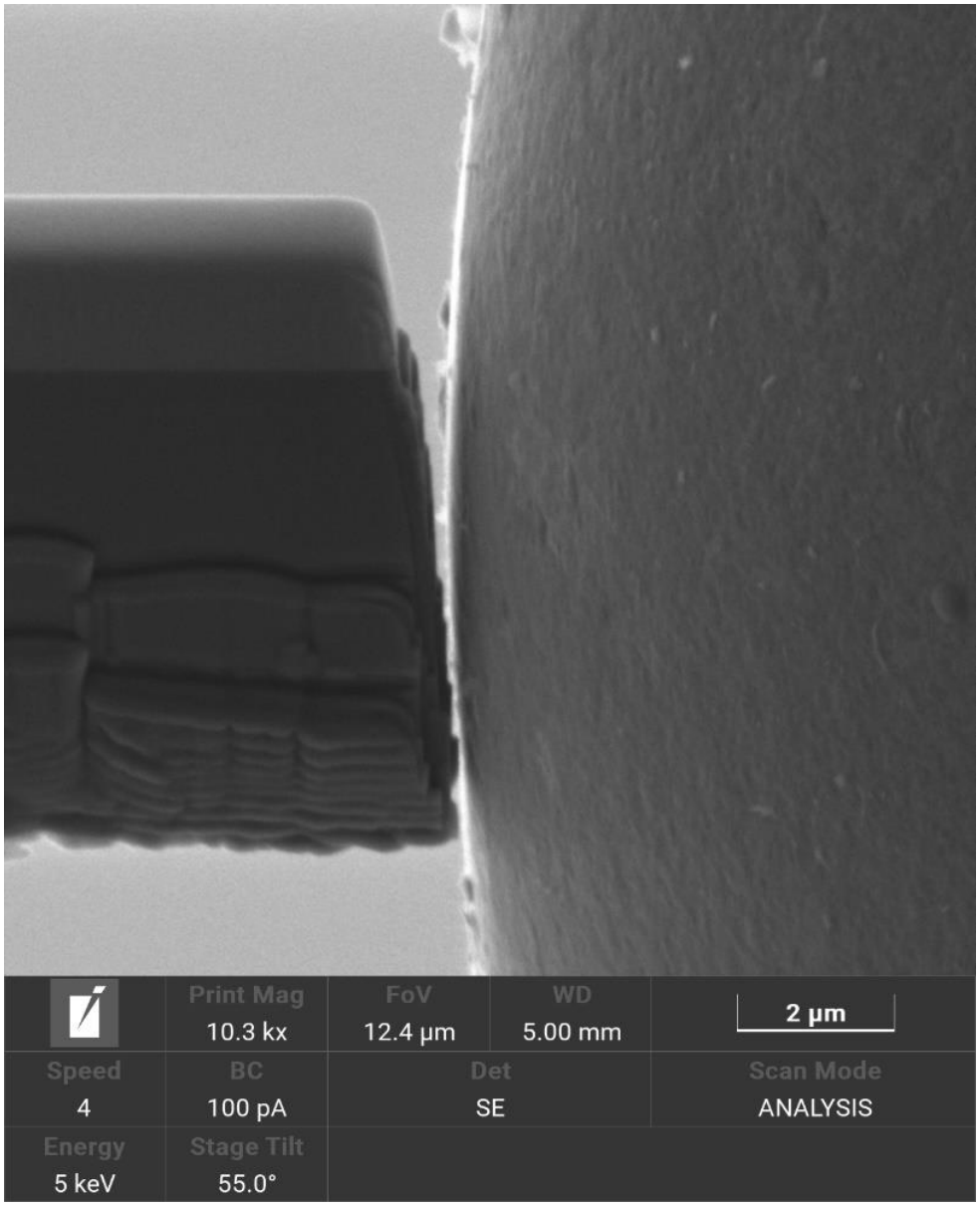

Fig. 48: *SEM image of the lamella almost touching the grid.*

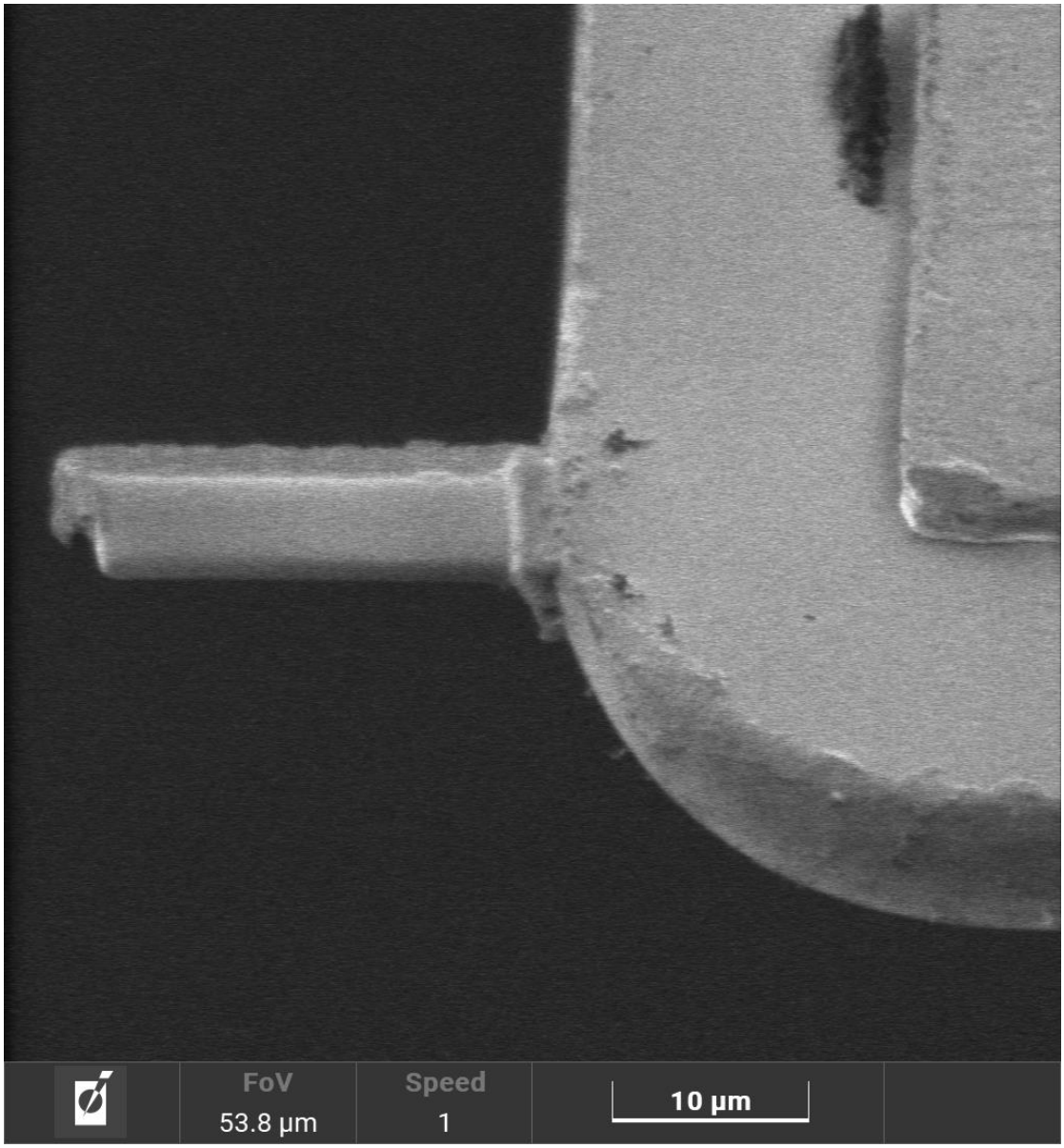

Fig. 49: *SEM image of the lamella after being weld to the grid.*

This process was done for both the chosen samples, with focus on the lines 4 and 7 of the G sample obtained in the previous chapter of the thesis.

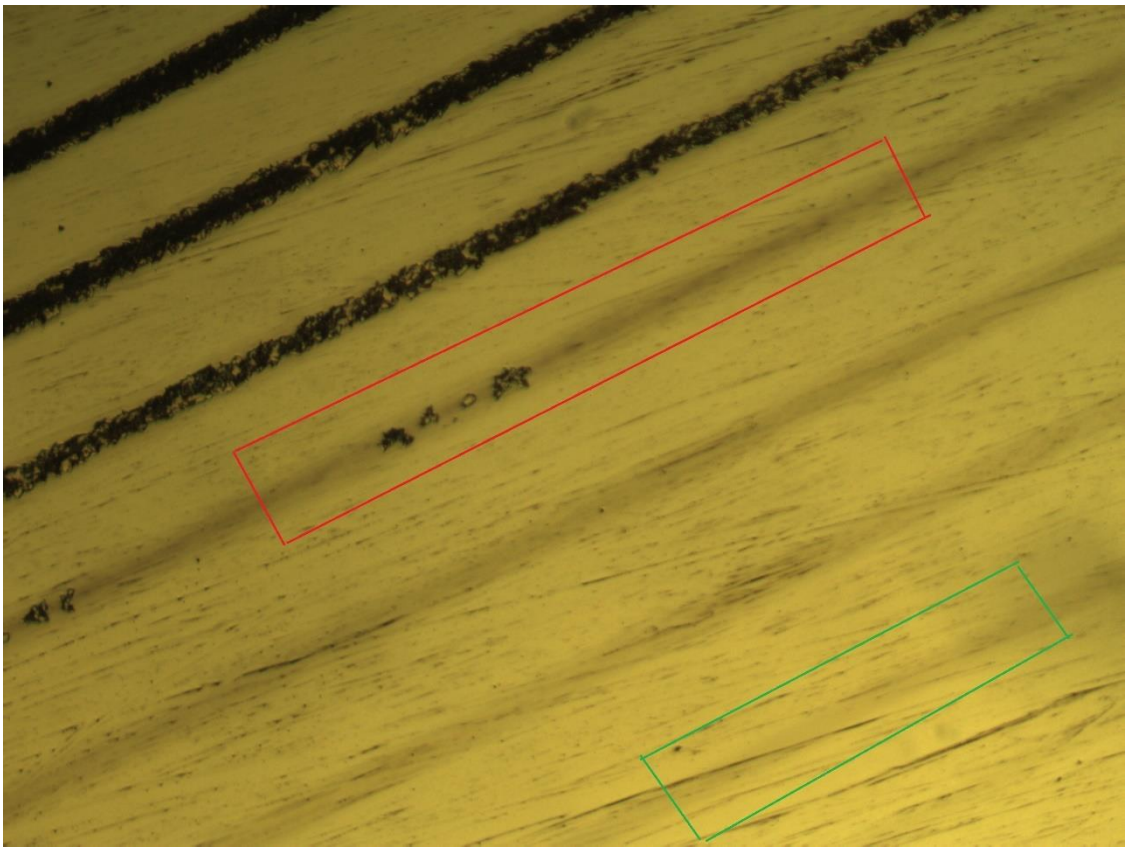

Fig. 50: *Lines 4 and 7 of sample's group G.*

Before moving to the TEM characterization, one more step is required, which is the **Thinning**.

4.3 Thinning process

This process is divided into 3 simple steps:

- High current 100 pA to achieve a first excavation of 2-3 μm.
- Low current of 20 pA to achieve thinning.

- Ion beam etching with low kilovolt voltage to reduce the amorphization factor.

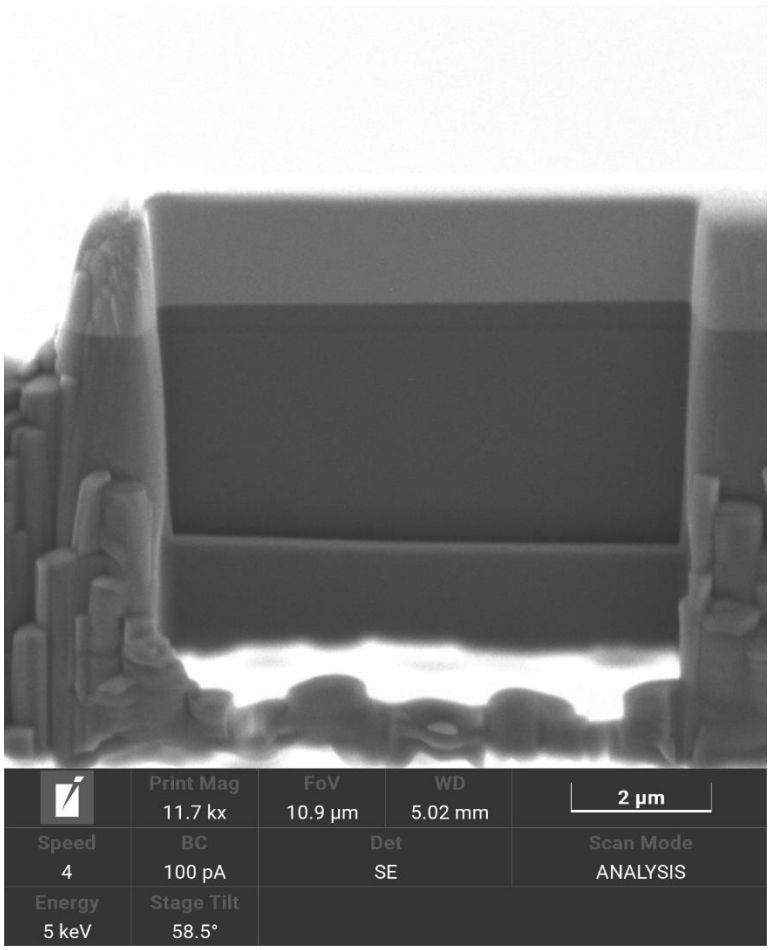

Fig. 51: *SEM image of the first two thinning steps.*

The last step is crucial since the amorphization layer needs to be as small as possible and the low voltage ion shower aims to reduces this layer enormously. We must remember that amorphization is a direct consequence of the destruction of the crystalline structure due to the ionic process and represents an unwanted layer in our analysis.

The final objective of this process is to achieve electronic transparency, which corresponds to a layer that is as thin as 50 nm. This is achieved by lowering in various etching steps the voltage of the ionic beam, going from 5 Kilovolt down to 2.

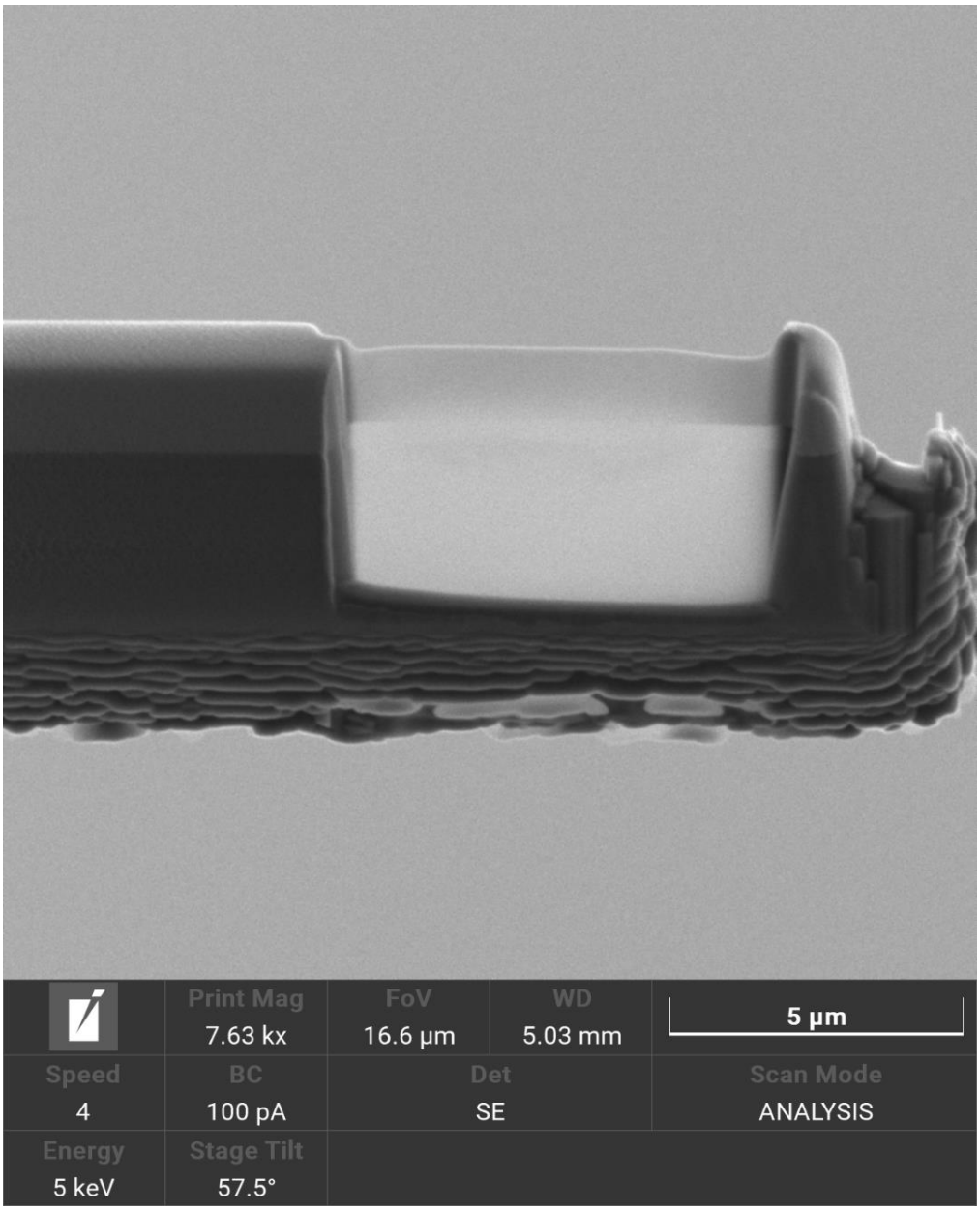

Fig. 52: *SEM image of the final product. The white part shows how efficiently the electronic transparency has been achieved.*

Analysis and characterization of the two lamellas has been done utilizing the TALOS F200XG2 with the High-resolution imaging mode.

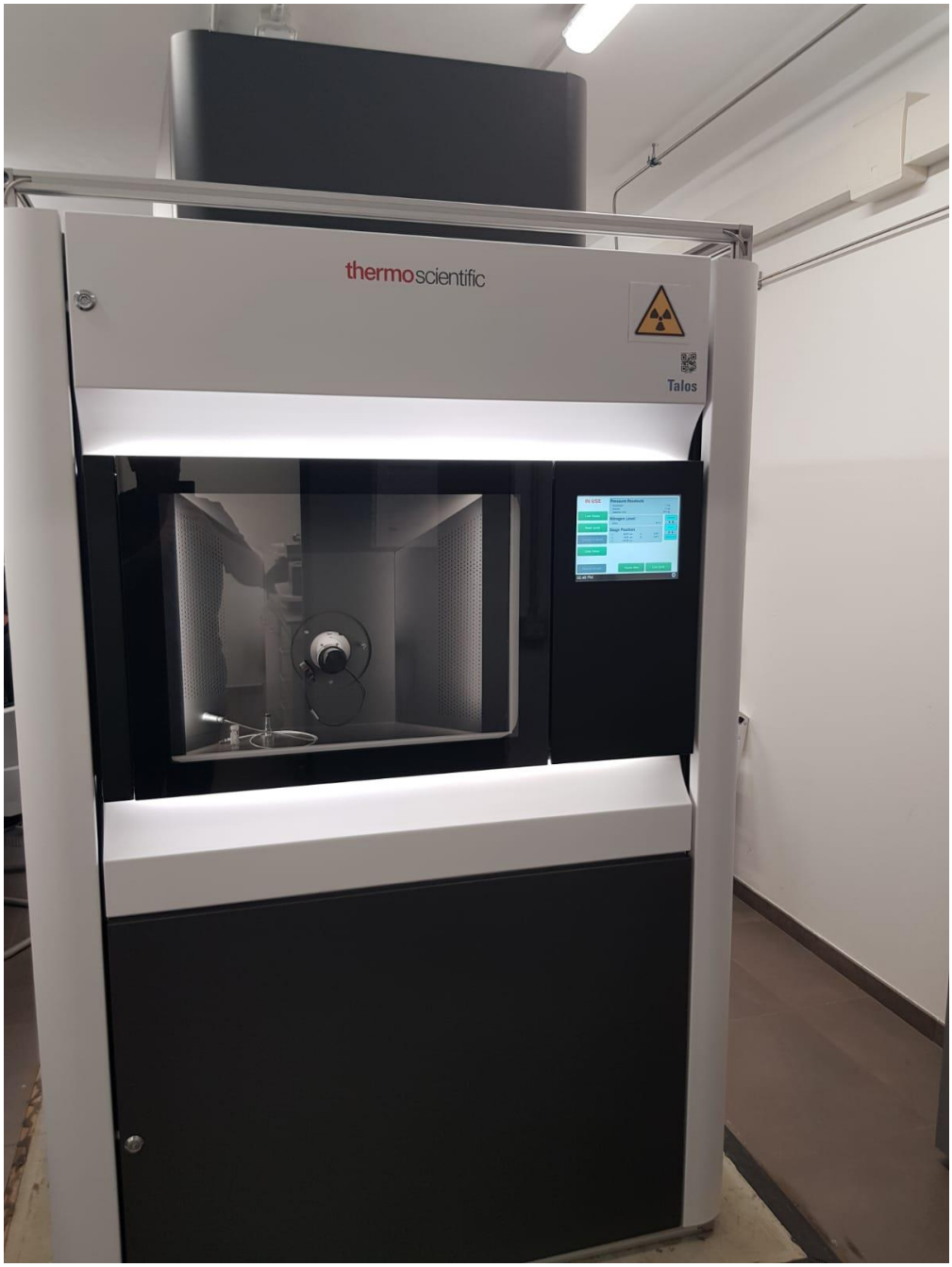

Fig. 53: *Talos F200XG2 model for Transmission Electron Microscopy.*

4.4 Transmission Electron Microscopy and EDX analysis

First, the specimen is loaded into the bore, using a small screw ring to hold the sample in place. The cartridge is then inserted into an airlock with bore perpendicular to the TEM optic axis.

Fig. 54: *Insertion of the cartridge into the TEM apparatus.*

Both the lamellas have been analysed with the Transmission Electron Microscopy showing the following results:

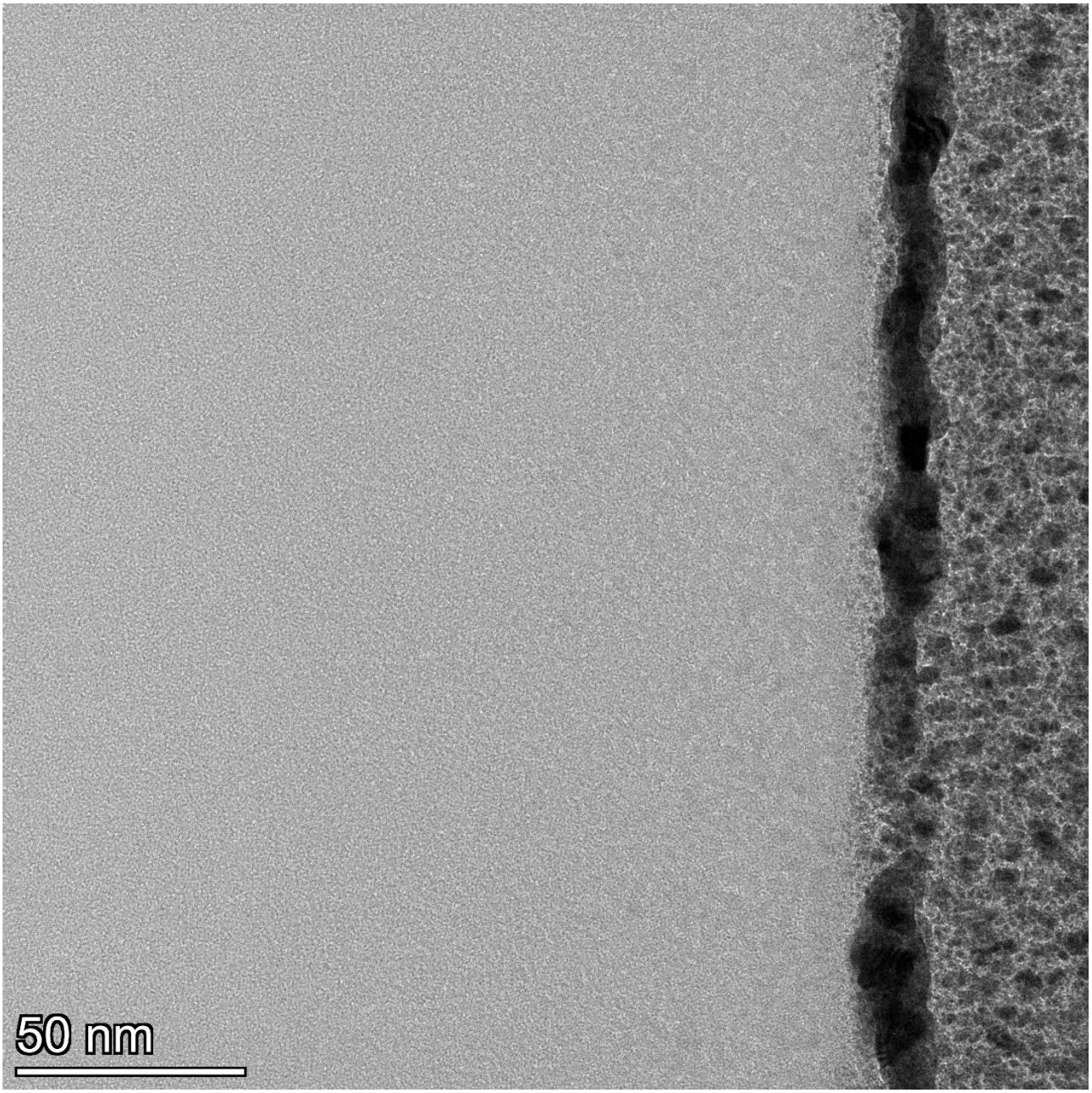

Fig. 55: *TEM image obtained in bright field configuration of the first lamella.*

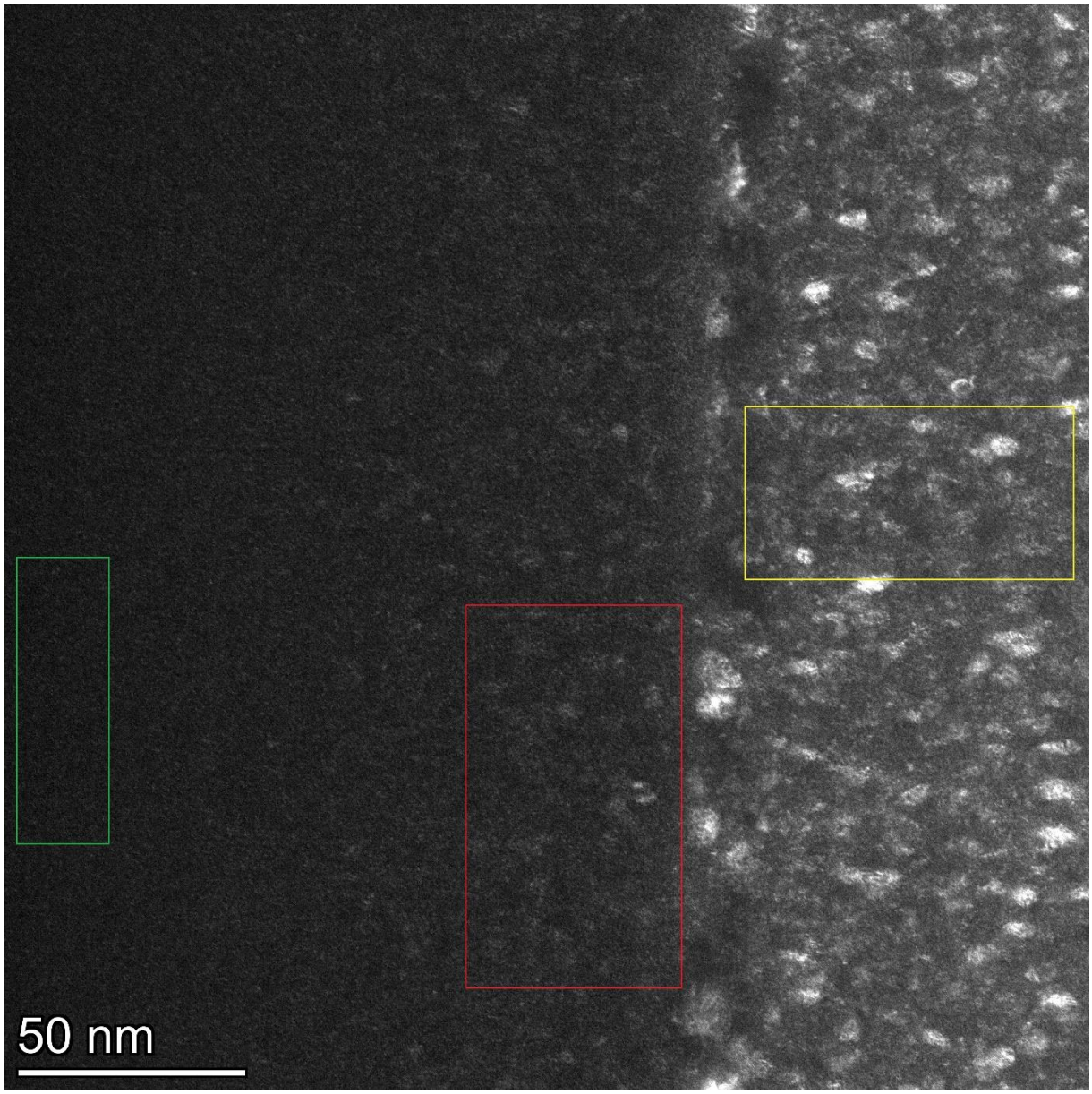

Fig. 56: *TEM image obtained in dark field configuration of the first lamella.*

The above images correspond to the fourth line coming from the annealed block G, previously seen in chapter 3.

In the dark field configuration, we can see the layer of platinum that was sputtered (yellow), on fig 57.

Since the lamella is very thin, more with respect to the second one, we incurred in some diffraction issues that arose especially during the sample alignment.

What came out was in fact that a very thin lamella would lead to complications regarding the alignment of the sample along a certain crystal orientation.

This had a physical repercussion, as it was shown by the formation of 'dunes', representing in fact the different crystal orientations.

A way to reduce the diffraction phenomenon is indeed to reduce the lens excitation. What's more is that from the live view registered with an exposition time of 200 ms (images are taken from the live video seen from the TEM's program) the crystalline domains scatters differently with respect to the substrate. By reducing the selected area at around two hundred nanometres and changing the TEM's configuration in the dark field one we can get valuable information.

In fact, looking at figure 57 we can see how the crystalline domains are indeed visible, with an achieved polycrystallinity of decent quality in the first fifty nanometres (red rectangle area).

Seems like the chosen parameters used to anneal the initial sample in chapter 3 where indeed quite effective but, in this case, it can also be possible to push even further the frequency and the duty cycle to try and reach an even higher value regarding the thickness of the polycrystalline layer that has been obtained up to now.

For the second lamella instead, the results were the following:

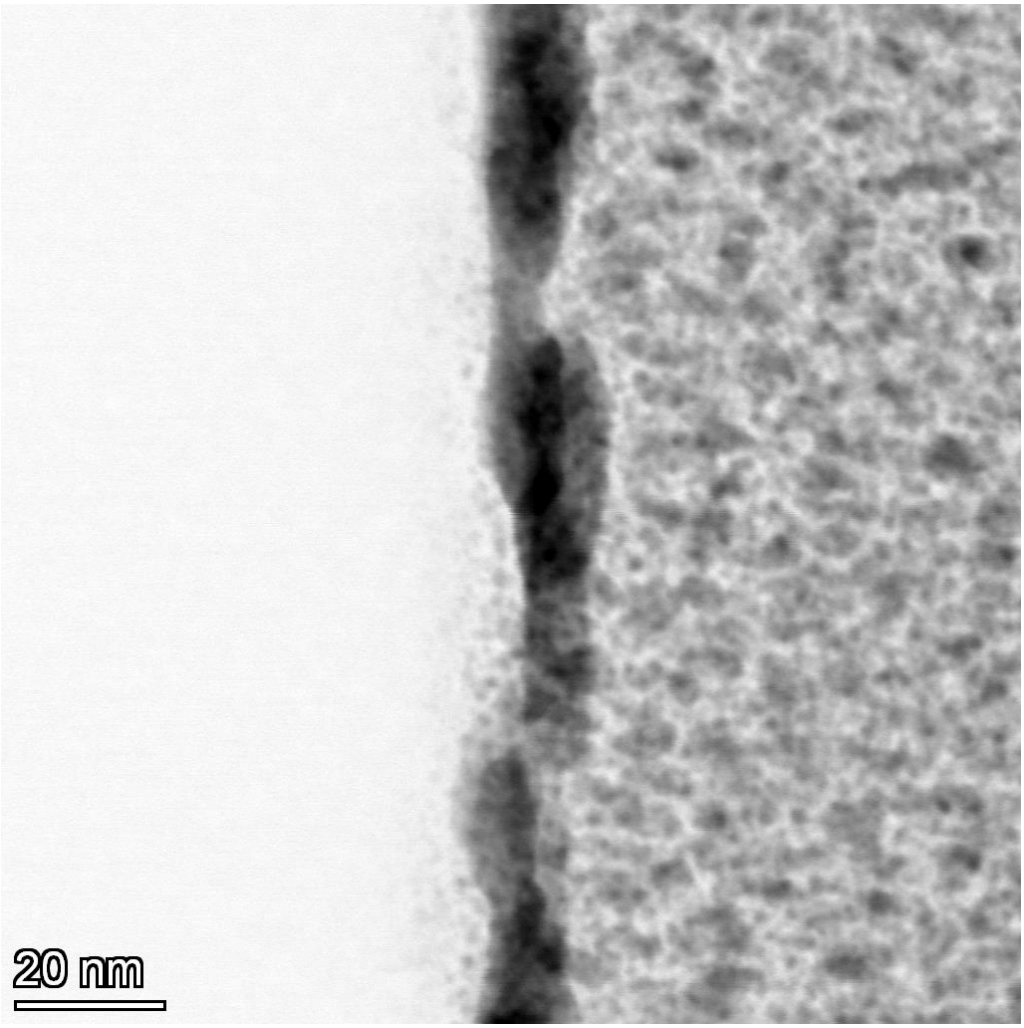

Fig. 57: *TEM image obtained in bright field configuration of the second lamella.*

From the bright field figure, it's possible to say that the crystalline substrate is well define and that the amorphization is reduced to a bare minimum (Much better with respect to lamella 1), meaning that the thinning process on this second lamella was much more efficient. This may be also related to having a thicker layer with respect to lamella 1.

The unwelcome news is that, by looking at the dark field configuration image, the crystalline domains are difficult to be evaluated since they are right below the sputtered platinum zone. In fact, due to the rugosity of the surface, the sputtered platinum slightly penetrated the material.

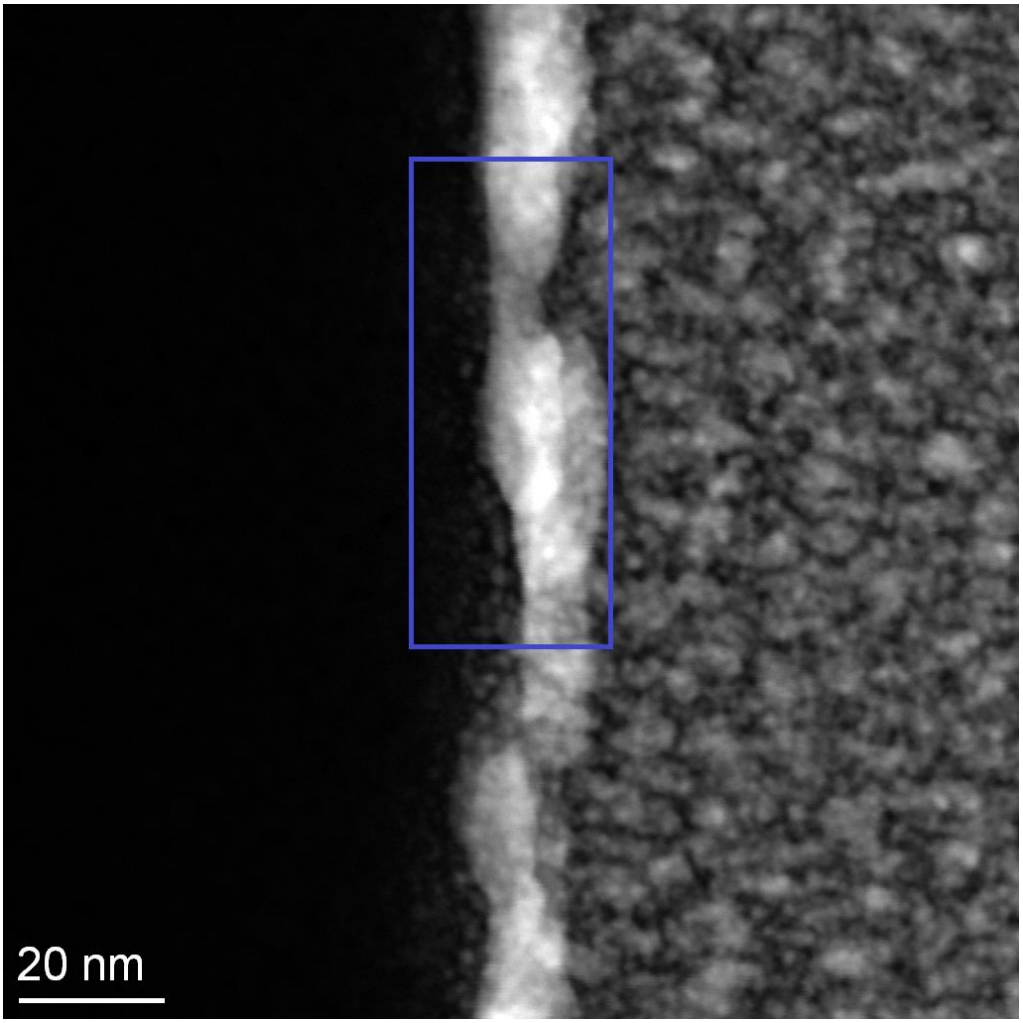

***Fig.58**: TEM image obtained in dark field configuration of the second lamella.*

The first supposition was that the length of the crystalline domain may have been of the order of just 5-6 nanometres and this due to the rugosity issue that was previously described.

To better understand if this crystallinity was correlated to the effective presence of polycrystalline SiC a STEM analysis with the EDX is indeed required.

Since up to now EDX has never been used except for this one time, the aim will be on giving a small introduction to this technique before giving full attention to the results which will come out thanks to it.

EDX (**Energy Dispersive X-ray Spectroscopy**) is a powerful analytical technique used to identify the elemental composition of a sample. It works by bombarding the sample with a focused electron beam, which causes the atoms in the sample to emit characteristic X-rays. These X-rays are then detected and analysed to determine the elements present in the sample and their relative concentrations.

The key components of an EDX system include:

- **Electron Source**: Typically, an electron gun or electron beam generator that produces a focused electron beam.
- **Sample Chamber**: Where the sample is placed for analysis.
- **X-ray Detector**: Detects the characteristic X-rays emitted by the sample.
- **Analyzer**: Processes the detected X-rays to determine their energy and intensity, which are used to identify the elements present.
- **Software**: Analyses the data and generates elemental composition reports.

The process involves scanning the electron beam across the surface of the sample and measuring the X-rays emitted at each point. By correlating the energy and intensity of these X-rays with known standards, the elemental composition of the sample can be determined. EDX is widely used in various fields including materials science, geology, forensics, and biology, to analyse the elemental composition of samples ranging from metals and minerals to biological tissues and environmental samples. It is particularly useful for non-destructive analysis, as it requires minimal sample preparation and can analyse samples in their natural state.

Another system is not required for the analysis since the TALOS F200XG2 already has incorporated in its system the choice of running an EDX analysis.

The results, seen in the next page are quite clear. In fact, by analysing the blue region from figure 60 it's clear how platinum prevails with an extremely high intensity (as it can be seen in the figure regarding the Spectra of the Area).

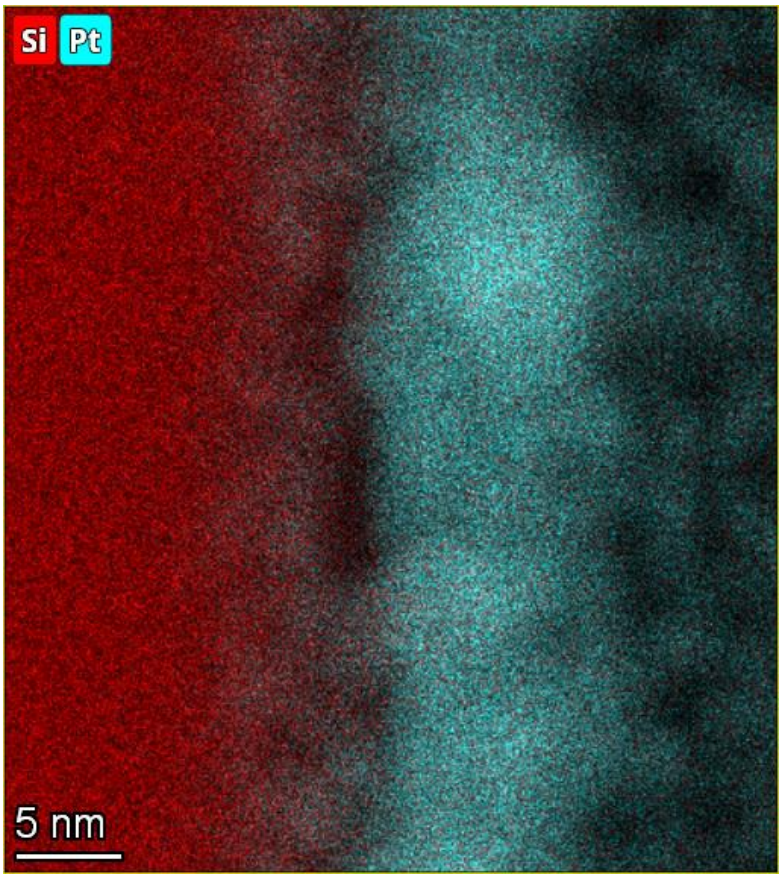

***Fig.59**: EDX analysis of the blue area, showing the main presence of Platinum in the crystalline interface.*

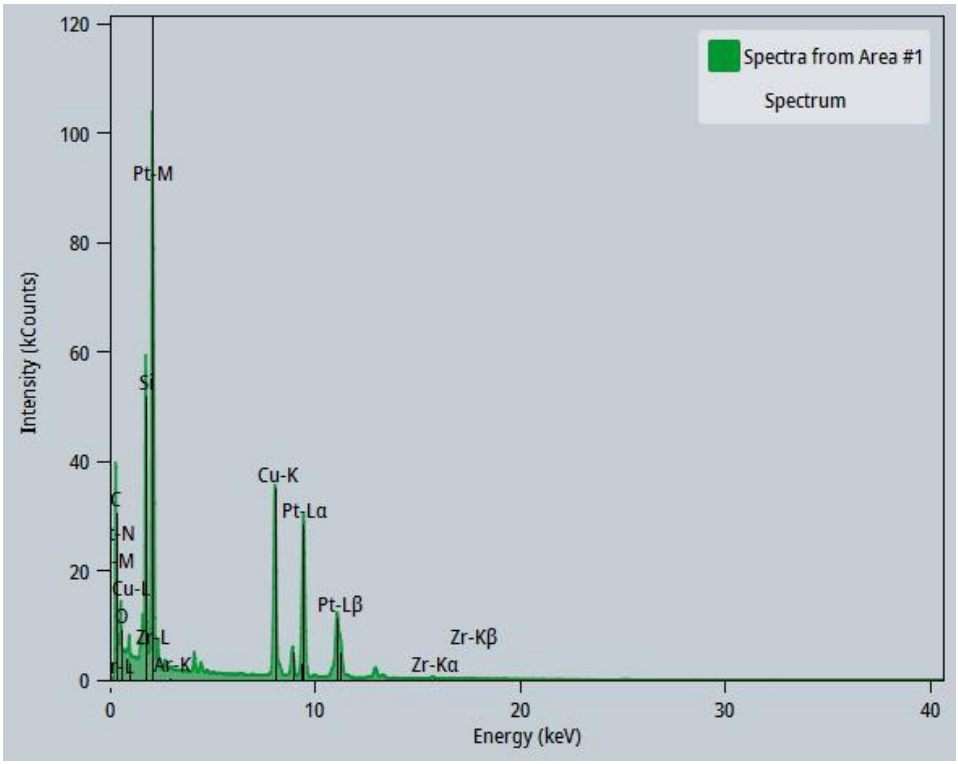

***Fig.60**: Spectrum obtained from the blue Area.*

This means that lamella two does not show any crystallinity that can be attributed to the laser annealing process that the SiC sample underwent from chapter 3.

An idea could be to use parameters, introduced in chapter 3, similar or with higher values of frequency or duty cycle so that it would be possible to not only crystallize another sample from its amorphous phase in the same way that we did to obtain the lamella 1, but also to achieve a much wider crystallization domain with respect to the one that we previously have seen during the TEM analysis of lamella 1.

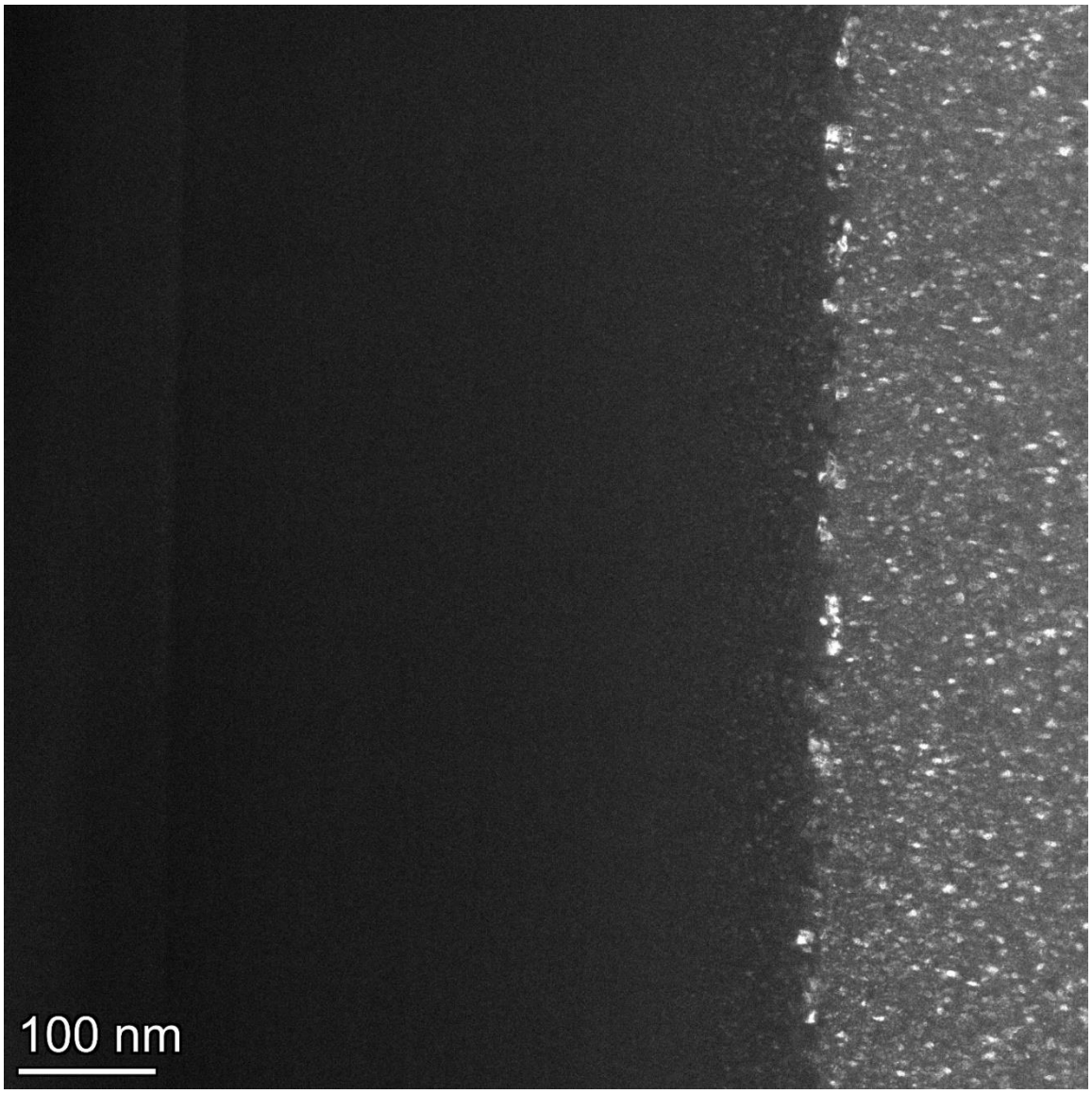

Fig. 61: *Full View of the TEM image obtained in dark field configuration of the first lamella with the 3 layers: Substrate, deposited SiC, sputtered Platinum.*

This analysis showed that Transmission Electron Microscopy is a well-rounded technique to characterize the laser annealed sample, time consuming and with high risks, since the preparation of the lamella features some steps in which particular care needs to be given, like the J-Cut or the approaching step of the lamella with the grid, which could both result in the loss of the lamella due to falloff. These high risks are well balanced by the resolution that the technique offers and, coupled with the EDX technology with which is possible to detect the main presence of the material on the selected area, they grant a good phase description of the crystalline structure of the SiC's topmost layer of the lamella.

Lamella 1 was indeed the one with more promising results, as it can be seen in figure 57 were the achieved polycrystallinity presents decent quality in the first fifty nanometres while for lamella 2 instead no crystallinity was detected.

This means that the choice of Frequency, Duty Cycle and Scanning Speed resulted to be quite efficient for lamella 1, while for lamella 2 higher values of these parameters are instead required.

Chapter 5 – Considerations and Conclusions

5.1 Considerations

The aim of this work of thesis is indeed to achieve the crystallization of an amorphous silicon carbide layer by laser annealing of the previously described sample in chapter 3. It's true that at the end of chapter 4, a crystallization of the surface amorphous layer of SiC has been achieved, even though the dimensions of the crystal domains obtained through laser annealing are of the order of 50 nanometres, still quite small. This can be considered initially as a good result, since by looking at the available scientific papers one can see for itself how not so many attempts at crystallizing the a-SiC layer were made with an UV laser.

The lack of scientific material that could have been used to confront the work done in the previous months is only one of the issues that have been observed. Some more common problems were:

- **Laser related**: What came out during the various annealing processes that have been done in the previous months is that the laser would sometimes not anneal properly and homogeneously the surface of the sample. Meaning that the average power would sometimes sway from it's calculated value. This could be related to a change in temperature of the laser; in fact, some tests were done regarding the turning off and on of the lasing device, showing how keeping the laser apparatus ON (not working) for more than a few hours would somehow affect its performance.

- **Human related**: Since this laser was the first UV laser to be used, I personally was not quite familiar at the beginning with the annealing process, with the settings of the parameters and the various steps required to ensure that a good annealing procedure could be achieved.

- **Analysis related:** As described in chapter 3, Raman Spectroscopy revealed to be a not so good technique for characterizing our sample since it was difficult to recognize

if the topmost a-SiC layer was crystallized or not, since the Raman Analysis Area would also comprehend the already crystalline 4H-SiC layer. In this case, time was also needed to search for a better characterization technique, which revealed to be Transmission Electron Microscopy, described theoretically in chapter 2 and which results are instead enlisted in chapter 4.

The first part of this work, related to the annealing of the test sample was required to gain confidence with the various steps of the workflow.

This first step was crucial to get a clear understanding of why the fibre laser didn't' have the correct parameters (especially the pulse width) to perform an annealing on the surface of the test sample that would not destroy the topmost amorphous layer and to test how the first three characterization techniques, Optical Microscopy, X-ray Diffraction and Raman Spectroscopy would behave with the test sample.

The introduction of the UV laser and removal of the test sample, substituted by the original Si-Si02-4H-SiC-aSiC structure would then lead to a complete change in the work process regarding both annealing, this time performed in a vacuum chamber, and characterization phase.

The characterization phase proved to be quite complicated at first, due to the Raman's limits on the new sample, bringing a change in the way where analysis was made.

This led to what described in chapter 4, the requirement to obtain a single lamella from the selected annealed lines on the sample shifted work on a new technique which was described in the beginning of chapter 4. By Coupling Scanning Electron Microscopy with Focus Ion Beam etching a couple of high-quality lamellas were obtained and then analysed by means of a Transmission Electron Microscope.

Results obtained were quite promising showing that, for certain values of Pulse Frequency, Duty Cycle and Scan speed, the laser annealing process on the amorphous SiC layer would produce crystal domains, showing a change from the a-SiC to its crystalline counterpart.

These crystal domains, even thou visible, do have small dimensions and regarding the thickness of the crystalline layer, it can be seen in fig. 57 how the obtained layer is not so ample.

5.2 Conclusions

A continuation of this work thesis could be centered in expanding this achieved crystalline layer by selecting from the various annealed samples the next new lines that are close to the already previously analysed ones in chapter 4.

Taking into consideration what has been said, since the first lamella previously described gave interesting results, it can be quick to think that the choice of the next lines would be coming from the lines that have a similar behaviour to line 4 of group G, highlighted in the next figure.

By rinsing and repeating this procedure it's possible to map and find the best possible values of Pulse Frequency, Scan Speed and Duty Cycle for which the crystal domains will result much wider than the first achieved one.

The lines seen in fig.62 are quite like the already analysed ones but present one different parameter value which is the Scanning Speed. Since reducing the scanning speed leads to an increase in the time in which a small portion of the sample undergoes laser annealing it could be an idea to check if this sample could present first the presence of crystalline domains and secondly if the dimension of these domains has increased or not.

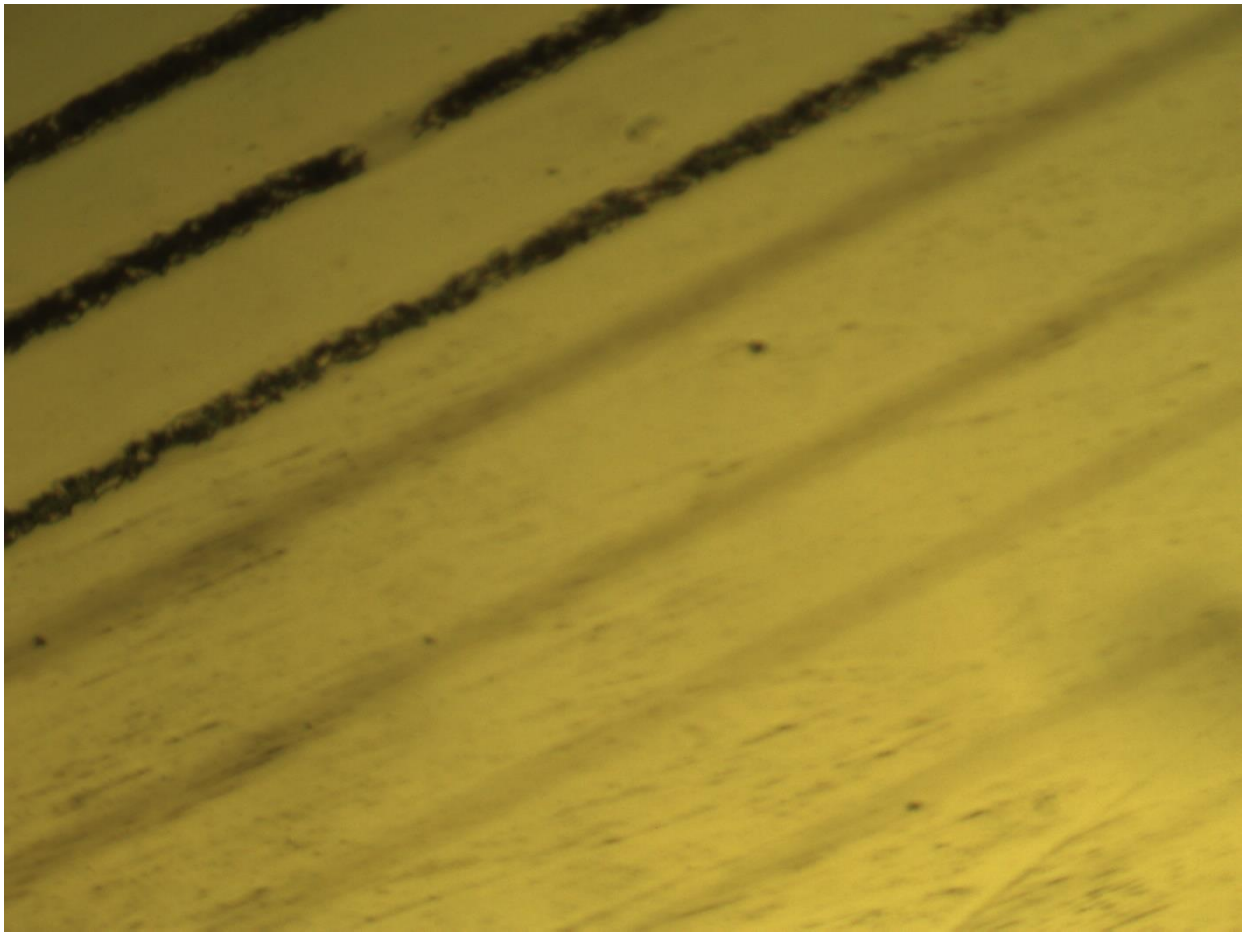

Fig. 62: *Image achieved with Leica's Optical microscopy enlighting possible line candidates to perform TEM analysis on. Parameters used are Frequency 70 Khz, Duty Cycle 40-80%, Scan Speed 90mm/s.*